Intestinal gluconeogenesis controls the neonatal development of hypothalamic feeding circuits

Judith Estrada-Meza, Jasmine Videlo, Clara Bron, Adeline Duchampt, Cécile Saint-Béat, Mickael Zergane, Marine Silva, Fabienne Rajas, Sebastien Bouret, Gilles Mithieux, et al.

Intestinal gluconeogenesis controls the neonatal development of hypothalamic feeding circuits

Authors

Judith Estrada-Meza[1*], Jasmine Videlo[1], Clara Bron[1], Adeline Duchampt[1], Cécile Saint-Béat[1], Mickael Zergane[1], Marine Silva[1], Fabienne Rajas[1], Sebastien G. Bouret[2], Gilles Mithieux[1#], Amandine Gautier-Stein[1*#]

Affiliations

[1] INSERM UMR-S1213, Université Claude Bernard Lyon 1, Lyon, France
[2] University Lille, Inserm, CHU Lille, Laboratory of development and plasticity of the Neuroendocrine brain, Lille Neuroscience & Cognition, Inserm UMR-S1172, Lille, France.
* Corresponding authors
# Co-last authors

Address for correspondence

Amandine Gautier-Stein

Permanent address: Université de Lyon, 7-11 rue Paradin, F-69008 Lyon, France

Tel: + 33 4 78 77 10 49

e-mail: amandine.gautier-stein@univ-lyon1.fr

and

Judith Estrada-Meza

Present address: Université de Lausanne, Department of Biomedical Sciences, Lausanne, Switzerland

e-mail: judith.estrada-meza@ens-lyon.org

Abstract

Objective: Intestinal gluconeogenesis (IGN) regulates adult energy homeostasis in part by controlling the same hypothalamic targets as leptin. In neonates, leptin exhibits a neonatal surge controlling axonal outgrowth between the different hypothalamic nuclei involved in feeding circuits and autonomic innervation of peripheral tissues involved in energy and glucose homeostasis. Interestingly, IGN is induced during this specific time-window. We hypothesized that the neonatal pic of IGN also regulates the development of hypothalamic feeding circuits and sympathetic innervation of adipose tissues.

Methods: We genetically induced neonatal IGN by overexpressing *G6pc1* the catalytic subunit of glucose-6-phosphatase (the mandatory enzyme of IGN) at birth or at twelve days after birth. The neonatal development of hypothalamic feeding circuits was studied by measuring Agouti-related protein (AgRP) and Pro-opiomelanocortin (POMC) fiber density in hypothalamic nuclei of 20-day-old pups. The effect of the neonatal induction of intestinal *G6pc1* on sympathetic innervation of the adipose tissues was studied via tyrosine hydroxylase (TH) quantification. The metabolic consequences of the neonatal induction of intestinal *G6pc1* were studied in adult mice challenged with a high-fat/high-sucrose (HFHS) diet for 2 months.

Results: Induction of intestinal *G6pc1* at birth caused a neonatal reorganization of AgRP and POMC fiber density in the paraventricular nucleus of the hypothalamus, increased brown adipose tissue tyrosine hydroxylase levels, and protected against high-fat feeding-induced metabolic disorders. In contrast, inducing intestinal *G6pc1* 12 days after birth did not impact AgRP/POMC fiber densities, adipose tissue innervation or adult metabolism.

Conclusion: These findings reveal that IGN at birth but not later during postnatal life controls the development of hypothalamic feeding circuits and sympathetic innervation of adipose tissues, promoting a better management of metabolism in adulthood.

Keywords: Intestinal gluconeogenesis; Neonatal period; Obesity; Hypothalamic development; Agouti-related peptide (AgRP); Pro-opiomelanocortin (POMC), Developmental programming

1. Introduction

The incidence of obesity and diabetes continues to increase at an alarming rate. In 2019, approximately 463 million adults were living with diabetes worldwide (International diabetes federations atlas), and 108 million children were obese in 2015 [1,2]. Diabetes and obesity are metabolic disorders that reflect the inability of the organism to appropriately metabolize its energy resources. This public health challenge drives a need to understand the factors implicated in the development of metabolic diseases. Epidemiological data, clinical studies and experimental research indicate that a deleterious nutritional environment during the perinatal period may exacerbate the susceptibility of an individual to develop metabolic diseases later in life, a concept known as the developmental origin of health and disease [3,4].

Key organs that regulate energy balance develop during gestation and continue their maturation during the first postnatal weeks in rodents. Thus, an inadequate perinatal environment can alter the development of the hypothalamus, which is a central regulator of energy balance [5–9]. The hypothalamus contains several nuclei, from which the arcuate nucleus of the hypothalamus (ARH) stands out as a central integrator of peripheral hormonal and nutritional cues. The ARH contains orexigenic neurons containing neuropeptide Y and the agouti-related peptide (NPY/AgRP neurons) and anorexigenic neurons containing the cocaine amphetamine-related transcript and pro-opiomelanocortin (POMC/CART neurons) [10–12]. These neurons transmit peptidergic signals through axons that project into other hypothalamic nuclei implicated in energy balance regulation such as the paraventricular nucleus of the hypothalamus (PVH), the dorsomedial hypothalamus (DMH) and the lateral hypothalamus (LH) [10,13].

It has been suggested that an optimal hypothalamic development is required for life-long regulation of energy balance [14]. Indeed, suboptimal hypothalamic development results in greater susceptibility to weight gain and insulin resistance induced by a high-calorie diet in adulthood [15,16]. In mice, ARH neuronal projections mainly develop during the first three postnatal weeks [17], notably under the influence of hormones that regulate feeding in the adult, such as leptin [18,19]. In rodents, plasma leptin levels surge from postnatal day 8 (P8) to P12 [20,21], and promote ARH AgRP and POMC axonal outgrowth in part by signalling through the long form of the leptin receptor (LepRb) and via the phosphorylation of signal transducer and activator of transcription 3 (STAT3) [18,22]. The developmental role of perinatal leptin extends to the innervation of peripheral organs such as the pancreas [23] and the adipose tissues [24,25].

Interestingly, the *de novo* production of glucose by the intestine (*i.e.* intestinal gluconeogenesis, or "IGN") also increases during the first two postnatal weeks in rats [26]. In adults, IGN controls a gut-brain neural circuit that is crucial for maintaining metabolic health [27,28]. Thus, mice lacking IGN develop a pre-diabetic phenotype [27], whereas mice with induction of IGN are protected from developing diabetes, obesity, hepatic steatosis and whitening of the brown adipose tissue (BAT) when fed a high-fat/high-sucrose diet (HFHS diet) [28]. Intestinal gluconeogenesis leads to the release of glucose into the portal vein, producing a "portal glucose signal" that activates hypothalamic neurons [29–32]. Interestingly, IGN promotes hypothalamic STAT3 phosphorylation independently of leptin [27,32]. Based on these observations, we hypothesized in addition to its regulatory action on feeding during adulthood, that IGN might regulate the development of ARH feeding circuits through STAT3 signalling and peripheral adipose tissue innervation during the neonatal period. We report that the neonatal induction of IGN controls axonal outgrowth of ARH AgRP and POMC neurons and sympathetic brown adipose tissue (BAT) innervation preventing the deleterious effects of a hypercaloric diet in adulthood.

2. Material and Methods

2.1 Animal models

We used only male mice. I.G6pc$^{overexp\text{-}P1}$ and I.G6pc$^{overexp\text{-}P12}$ male mice were obtained by crossing Rosa26$^{Stopcassette\text{-}lox\text{-}G6pc}$ with Villin-CRE^{ERT2} mice, I.G6pc$^{overexp\text{-}c}$ were obtained by crossing with Villin-CRE mice, in a C57Bl/6J genetic background. Litters were balanced to 7-9 pups per dam. To induce *G6pc1* overexpression in I.G6pc$^{overexp\text{-}P1}$ and I.G6pc$^{overexp\text{-}P12}$ mice, half of pups received an intra-gastric injection of tamoxifen (20 µg, Sigma-Aldrich) at postnatal day 1 (P1) or P12. The other half was injected intra-gastrically with 20 µL of tamoxifen's vehicle, sunflower oil at P1 or P12 (the controls), respectively [33]. Male wild-type mice (C57Bl/6J, Charles River Laboratories, France) were also used, and followed the same tamoxifen or vehicle treatment previously described. All mice were group housed in the animal facility of Lyon 1 University (*Animalerie Lyon Est Conventionnelle*) under controlled temperature conditions (22°C), with a 12 hours light/12 hours dark cycle. Mice had *ad libitum* access to water and to a standard chow diet (A04 ; SAFE; Augy, France) until the 6th week of life, when the diet was switched to a high-fat/high-sucrose diet (HFHS diet) (consisting of 36.1% fat, 35% carbohydrates (50% maltodextrine + 50% sucrose), 19.8% proteins) [27]. All procedures were performed in accordance with the principles and guidelines of the European

Convention for the Protection of Laboratory Animals. The regional animal care committee (CEEA-55, Lyon 1 University, France, APAFIS #11845) approved all the experiments presented.

2.2 Food Intake and Body Weight Measurements

During the perinatal period, mouse pups were weighted at P7, P11, P15 and P20.

Body weight and food intake were measured once and twice per week, respectively, since weaning. Food intake was also measured individually over 72 hours in a calorimetric cage.

2.3 Glucose and Insulin Tolerance Tests

Blood glucose levels were measured, and glucose and insulin tolerance tests were performed after 4 and 5 weeks of HFHS diet, respectively, in 6h fasted mice, as previously described [34]. Briefly, mice were injected with 1 g of glucose per kg body weight for GTT, and 0.75 U of insulin per kg body weight for ITT, intraperitoneally. Blood was withdrawn from the tail vein at indicated times for glucose and/or insulin assessment. Blood glucose was measured using an "Accu-Chek Go" glucometer (Roche Diagnostics).

2.4 Body Composition and Metabolism Studies

After 6 weeks of HFHS diet, fat and lean mass were determined with nuclear magnetic resonance spectroscopy (Minispec LF90 II; BRUKER Society; ANR-11-EQPX-0035 PHENOCAN). After 7 weeks of HFHS diet, calorimetry parameters were measured during 72h. Oxygen consumption and carbon dioxide production were determined using a single chamber system and used for the calculation of energy expenditure (Phenomaster, TSE Systems GmbH). All procedures were performed on individually housed mice by the ANIPHY platform, SFR Lyon-Est from Lyon 1 University.

2.5 Blood and tissue sampling and plasma analyses

Mouse pups were taken from dams at different ages and decapitated. For the leptin sensitivity test, mouse pups were decapitated 30 minutes after an intraperitoneal injection of 0.003 mg/g leptin (Enzo Life Science). Adult mice were killed after 8 weeks of HFHS diet by cervical dislocation after a 6h fast. Tissues were immediately removed, frozen in liquid nitrogen, and kept at −80°C. Blood was withdrawn from the trunk when mouse pups were decapitated, or from the submandibular vein from 6h fasted adult mice, then collected in ethylene diamine

tetraacetic acid (EDTA) and conserved at -80°C. Insulin and leptin were assayed using insulin (Mercodia, ref. #10-1247-01) and leptin (Enzo, ref #ADI-900-019A) mouse ELISA kits.

2.6 Adipose tissue staining

Inguinal WAT and epididymal WAT were dissected and put in formol for 24h, then incubated in PBS 1X. 3 µm sections were cut and tissues were stained with hematoxylin and eosin by the CIQLE platform, SFR Lyon-Est from Lyon 1 University.

2.7 Gene expression analysis

The first 2cm piece of the proximal jejunum was homogenized with the Fast Prep® system and total RNAs were isolated from tissues with the TRIzol reagent protocol (Invitrogen). Reverse transcription was performed on 1 µg of mRNA using the Qiagen QuantiTect Reverse Transcription kit. Real-time qPCRs were performed using sequence-specific primers with Takyon™ No Rox SYBR® MasterMix dTTP Blue (Eurogentec). The expression of mRNAs was normalized to the mouse ribosomal protein L32 transcript expression using the 2- $\Delta\Delta C_t$ method.

G6PC1: Fw: TTACCAAGACTCCCAGGACTG ; Rev: GAGCTGTTGCTGTAGTAGTCG

UCP1: Fw: TACCAAGCTGTGCGATGT ; Rev: AAGCCCAATGATGTTCAGT ; Ribosomal protein L32: Fw: CAAGGAGCTGGAGGTGCTGC; Rev: CTGCTCTTTCTACAATGGC

2.8 Glucose-6-phosphatase enzymatic activity

The second 2 cm piece of the proximal jejunum was treated similarly to tissues treated for gene expression analyses. The glucose-6-phosphatase (G6Pase) activity was measured as previously described [26]. Briefly, all the tissue (around 20 mg for pups and 100 mg for adults) was homogenized in 9 volumes of Hepes Sucrose before G6Pase activity was measured. The specific G6Pase activity was subtracted from total phosphatase activity. The results are expressed as micromoles of hydrolyzed substrate per minute.

2.9 Immunofluorescence assays

Brain fixation of mice aged of 20 or 80 days was conducted as previously described [32]. Fixed brains were frozen for 1 min. in C_5H_{12} at -40°C, and 40 µm sections were cut at -25°C. Sections were kept in PBS/0.25% NaN_3 until processed for immunofluorescence. We chose one free-floating section per hypothalamic nucleus of interest with a loop. Briefly, we carried out 3 PBS 1X-Tx0.4% washes, incubated the sections in 10mM citric acid pH 6.0 for 20 min at 80°C, and

saturated (PBS1X-Tx0.4%, BSA 5%, goat serum 5%) for 2-4h at room temperature (RT). Incubation with primary antibodies (Rabbit AgRP 1/4000 and POMC 1/10000, Phoenix Pharmaceuticals; P-STAT3 1/3000, Cell Signaling, #9145) was done during 2 or 1 night, respectively, at 4°C, followed by incubation with secondary antibodies (Goat α-rabbit IgG Alexa fluor 488, 1/500, Life Technologies) for 2h at RT, and Hoescht 33342 (1/5000) for 5 min. Sections were washed 3X and mounted with Life ProLong Gold antifade reagent (Life Technologies). All photographs were taken with an objective 20X (0,8 M27) DIC using a confocal miscrocope Zeiss LSM 880 Airyscan NLO.

2.10 Fiber density quantitative analyses

A single image corresponding to the central position in the Z-plane of each nucleus of interest was acquired with an objective 20X (0,8 M27) DIC using a confocal miscrocope Zeiss LSM 880 Airyscan NLO. Image file names were coded prior to quantification to ensure non-biased treatment. Quantification was performed with Image J. For quantitative analyses of AgRP and POMC fiber densities in each hypothalamic nucleus of interest, the area of quantification was selected manually as a region of interest (ROI). Quantification was performed on a manually thresholded image (allowing separation of immunoreactive fibers from the background). We divided the integrated density value (which reflects the sum of pixels in the thresholded image) by the area of the ROI. For quantitative analyses of POMC cell bodies in the ARH, POMC-immunoreactive cell bodies were manually counted. Only one image was quantified per hypothalamic nucleus and per mice.

2.11 Western blot analyses

Western blot analyses were performed on whole hypothalamus or adipose tissue samples as previously described [35]. Briefly, whole cell extracts from tissues were lysed in standard lysis buffer at 4°C. Aliquots of 30 µg proteins were separated by 9%-SDS polyacrylamide gel electrophoresis and transferred to PVDF Immobilon membranes (Millipore). After saturation, the membranes were probed with primary antibodies and then with goat secondary anti-rabbit IgG linked to peroxidase. Chemiluminescent signals were acquired with the Chemidoc Imaging System (Biorad) and quantified using Image Lab software (Biorad). Primary antibodies: P-STAT3 and STAT3 (1/2000, Cell Signaling, #9145 and #4904, respectively), tyrosine hydroxylase (TH)(1/1000, Cell Signaling #588455), AgRP (1/1000, Interchim, #AGRP11-S), POMC (1/1000, Cell Signaling, #23499). Secondary antibodies: goat α-rabbit IgG linked to peroxidase (1/1000, Biorad). Stain-free gels were used (Biorad, ref. #1610181).

2.12 Lactation

Mouse pups aged of 7, 11 and 15 days were separated from dams during 2h and weighted. Pups were then reunited with dams for 1h, after which pups were weighted again. The difference between both weights was considered as milk lactated by pups.

2.13 Statistical analyses

Results are reported as means ± standard error of the mean (SEM). Normal distribution was verified for all analyses. Two-group comparisons were analysed using unpaired t-tests. The effect of two independent variables on a dependent variable was analysed using two-way ANOVA, followed by multiple comparisons, and corrected for multiple comparisons with a SIDAK test. The differences were considered statistically significant at *$p<0.05$, **$p<0.01$ and ***$p<0.001$. Statistical details of experiments can be found in the figure legends. Statistical analyses were performed with GraphPad Prism 6 software. CalR was used for supplemental Fig. 6 [36].

3. Results

3.1 Neonatal induction of intestinal gluconeogenesis

Glucose-6-Pase enzyme and more precisely its catalytic sub-unit encoded by *G6pc1* is mandatory for endogenous glucose production. We previously reported a peak in *G6pc1* mRNA expression and G6Pase activity reflecting IGN in rat neonates [26]. We first confirmed that a peak of intestinal *G6pc1* mRNA expression and G6Pase activity also occurred at P5 in C57Bl/6J mice (Fig. 1a). To assess the function of IGN during the neonatal period, we used a CRE/lox strategy to develop a murine model with an inducible and intestine-specific overexpression of *G6pc1*. We used the previously described mouse model Villin$^{CRE\text{-}ERT2}$.Rosa26$^{Stopcassette\text{-}lox\text{-}G6pc}$ expressing the complementary DNA sequence of *G6pc1* in the Rosa26 locus positioned after a STOP cassette flanked with loxP sequences and CRE^{ERT2} under the control of the *Villin* promoter [28]. An injection of tamoxifen leads to the activation of the CRE^{ERT2} recombinase in *Villin*-expressing cells thereby leading to the excision of loxP sequences and permitting intestinal overexpression of *G6pc1* [37] (Fig. 1b). First, we induced the intestinal *G6pc1* overexpression in male pups by injecting tamoxifen at P1 (I.G6pc$^{overexp\text{-}P1}$ mice). The deletion of the STOP cassette was specific of the intestine of I.G6pc$^{overexp\text{-}P1}$ pups and persisted during adulthood (Fig. 1c). I.G6pc$^{overexp\text{-}P1}$ pups exhibited a 2.5 to 5-fold increase of *G6pc1* expression

from P3 (Fig. 1d), and a continuous 1.3 to 2-fold increase of intestinal G6Pase activity from P5 in comparison to control mice (Fig. 1e).

3.2 Rewiring of hypothalamic AgRP and POMC fibers in mice with a neonatal induction of IGN

Hypothalamic feeding circuits that project from the arcuate nucleus (ARH) to other hypothalamic nuclei involved in the regulation of energy balance develop mainly during the first two weeks of postnatal life in rodents, and show an adult-like innervation pattern around P16 [17]. To determine whether neonatal IGN plays a role in the development of hypothalamic feeding circuits, we immunolabeled AgRP and POMC fibers in brain sections of P20 I.G6pc$^{overexp\text{-}P1}$ and control mice. I.G6pc$^{overexp\text{-}P1}$ pups exhibited approximately 35% more AgRP-immunoreactive fibers in the anterior part of the hypothalamic paraventricular nucleus of the hypothalamus (PVHant) in comparison to control littermates (Fig. 2a-b). However, normal densities of AgRP-immunoreactive fibers were found in the posterior part of the paraventricular nucleus of the hypothalamus (PVHpost), the lateral hypothalamus (LH) and the DMH (Fig. 2a-b). In addition, I.G6pc$^{overexp\text{-}P1}$ pups exhibited a 20% reduction of POMC-immunoreactive fibers in the PVHant, whereas no differences were observed in the other nuclei (Fig. 2a-c). These modifications were not associated with a difference in the quantity of AgRP or POMC proteins (Supplemental Fig. 1a,b), suggesting that they are not due to a reduced expression of the neuropeptides. However, I.G6pc$^{overexp\text{-}P1}$ mice showed a decrease in the number of ARH POMC neurons (Supplemental Fig. 1c). Because previous studies reported that tamoxifen could impact neurons involved in reproduction [38,39], we also verified whether neonatal tamoxifen administration to wild-type pups affect the density of AgRP or POMC fibers. Tamoxifen administration to P1 wild-type pups did not affect the density of AgRP or POMC fibers in any of the studied hypothalamic nuclei (Supplemental Fig. 2) but decreased the number of ARH POMC neurons (Supplemental Fig. 1c). To distinguish the effect of intestinal *G6pc1* induction from the effect of tamoxifen injection at P1, we also performed an experiment in I.G6pc$^{overexp\text{-}c}$ mice in which *G6pc1* was induced constitutively without tamoxifen treatment. In this model, no change in AgRP-immunoreactive fibers was found between I.G6pc$^{overexp\text{-}c}$ mice and their littermates. However, we measured a 50% decrease of POMC-immunoreactive fibers in the PVHant of I.G6pc$^{overexp\text{-}c}$ mice compared to their littermates (Fig. 3a-c), suggesting that a constitutive induction of intestinal *G6pc1* leads to a reorganization of POMC fiber connections to the PVHant. Importantly, the decrease in PVHant POMC fibers was not associated with a decrease in ARH POMC neurons in I.G6pc$^{overexp\text{-}c}$ mice

(Supplemental Fig. 1c). These results suggest that the reduction in the number of ARH POMC neurons in I.G6pc$^{overexp-P1}$ mice is likely attributable to the tamoxifen injection at P1. Therefore, the neonatal induction of intestinal *G6pc1* appears to regulate PHVant fiber outgrowth independently of both ARH POMC neuron numbers and ARH POMC or AgRP protein levels. Our results indicate that there is a difference in the density of POMC and AgRP fibers in I.G6pc$^{overexp-P1}$ mice at P20. To determine whether it persisted throughout life, we examined whether the effects on fiber density observed in the PVHant of I.G6pc$^{overexp-P1}$ pups were also found in adult mice. The density of AgRP- and POMC-immunoreactive fibers were similar between adult I.G6pc$^{overexp-P1}$ mice and control littermates (Supplemental Fig. 3), suggesting a catch up of both AgRP and POMC fiber's growth between P20 and adulthood.

Altogether, these data suggest that, during the neonatal period, IGN controls the wiring of AgRP/POMC fibers projecting to the PVHant, which could be compensated later in life.

3.3 The effect of IGN on hypothalamic AgRP and POMC fibers is restricted to the neonatal period

To investigate whether the effects associated with the neonatal induction of intestinal *G6pc1* are restricted to the neonatal period, we induced intestinal *G6pc1* at P12 in male pups (I.G6pc$^{overexp-P12}$ mice), right after the endogenous neonatal peak of IGN. Strikingly, in contrast to I.G6pc$^{overexp-P1}$ pups, P20 I.G6pc$^{overexp-P12}$ pups had AgRP and POMC fibers density similar to controls in all studied nuclei (Fig. 4a-c). Importantly, the administration of tamoxifen to P12 wild-type pups did not alter AgRP or POMC fiber density (Supplemental Fig. 4). These data suggest that IGN controls the development of AgRP and POMC neural projections to the PVHant during a critical period restricted to the first two weeks of postnatal life.

3.4 Control of hypothalamic STAT3 phosphorylation and leptin sensitivity by neonatal IGN in mouse pups

The neonatal leptin surge, which occurs from P8 to P12, is critical for the proper outgrowth of AgRP and POMC neurites [18,19]. To investigate this, we analyzed the leptin surge in I.G6pc$^{overexp-P1}$ mice and their control littermates. While the leptin surge still occurred at P9, its magnitude was reduced in I.G6pc$^{overexp-P1}$ pups compared to their littermates (Fig. 5a). Neonatal leptin promotes outgrowth of AgRP and POMC axons in part through STAT3 phosphorylation [22]. We thus measured plasma leptin and hypothalamic STAT3 phosphorylation levels at P9, which corresponds to the neonatal leptin peak. At P9, I.G6pc$^{overexp-P1}$ mouse pups had the same amount of STAT3 phosphorylation levels in the hypothalamus as their control littermates (Fig.

5b, e-f) despite lower leptin levels (Fig. 5a) . Interestingly, STAT3 phosphorylation levels in the hypothalamus of P9 mouse pups were correlated to intestinal *G6pc1* expression but not to leptin levels (Fig. 5c-d). Additionally, after an intra-peritoneal leptin injection, P20 I.G6pc$^{overexp-P1}$ mouse pups showed a tendency to higher STAT3 phosphorylation than their control littermates, suggesting greater sensitivity to leptin (Fig. 5g). Taken altogether, our results suggest that the neonatal induction of intestinal *G6pc1* at P1 controls AgRP and POMC fibers outgrowth by promoting STAT3 phosphorylation independently of plasma leptin levels and/or by promoting hypothalamic leptin sensitivity.

3.5 Mice with a neonatal induction of IGN exhibit improved energy balance under a hypercaloric diet

Previous studies have reported that abnormal development of AgRP and POMC neuronal projections during the neonatal period can have consequences on adult metabolism [8,40,41]. We first investigated whether the neonatal induction of intestinal *G6pc1* affects body weight, milk intake, and glycaemia during the neonatal period. I.G6pc$^{overexp-P1}$ pups showed control-like weight, milk intake and even glycaemia (Supplemental Fig. 5), despite having increased intestinal glucose production. In addition, plasma insulin levels were equivalent in both P9 G6pc$^{overexp-P1}$ and control littermates (Control: 0.52±0.06 vs. I.G6pc$^{overexp-P1}$: 0.44±0.13 µg/mL). Next, to uncover the role of the neonatal induction of intestinal *G6pc1* on metabolism of adult mice, we challenged I.G6pc$^{overexp-P1}$ mice and control littermates with a HFHS diet starting at 6 weeks of age and for two months. A HFHS diet is known for altering weight gain, glucose homeostasis and adiposity in C57Bl/6J mice. After two months on a HFHS diet, I.G6pc$^{overexp-P1}$ mice were 23% lighter compared to control mice (Fig. 6a) despite a comparable food intake (Control: 1.816±0.404; I.G6pc$^{overexp-P1}$: 2.158±0.109 g/day). In line with their decreased weight gain, I.G6pc$^{overexp-P1}$ mice exhibited 30% reduction in body fat mass (Fig. 6b) and a 10% increase in body lean mass in comparison to control littermates (Fig. 6c). Moreover, I.G6pc$^{overexp-P1}$ mice also showed an increase in energy expenditure (Fig. 6d). The increase in energy expenditure was not associated with an increase in locomotor activity (Supplemental Fig. 6). Importantly, the administration of tamoxifen *per se* does not affect the body composition of male mice [42]. I.G6pc$^{overexp-P1}$ mice also had a discrete improvement in glucose tolerance compared to control mice (Fig. 6e), a trend for improved insulin tolerance (Fig. 6f), but no difference in insulinemia (Fig. 6g). However, we cannot definitively attribute the improved protection of glucose homeostasis specifically to the induction of *G6pc1*, as the potential effects of tamoxifen administration at P1 cannot be excluded. Notably, adult male

mice injected with tamoxifen at P1 exhibited a modest increase in insulin tolerance [42]. Importantly, the I.G6pc$^{overexp\text{-}P1}$ phenotype recapitulated the beneficial metabolic effects induced by a constitutive induction of intestinal *G6pc1*. Indeed, we previously demonstrated that adult mice with a constitutive induction of *G6pc1* (I.G6pc$^{overexp\text{-}c}$) had reduced weight gain, higher energy expenditure and improvement in glucose tolerance compared to WT mice when fed a HFHS diet [28,35].

High circulating leptin levels and hypothalamic leptin resistance, illustrated by decreased hypothalamic P-STAT3, are hallmarks of obesity [43–46]. I.G6pc$^{overexp\text{-}P1}$ mice displayed reduced plasma leptin levels (Fig. 6h) and exhibited increased hypothalamic STAT3 phosphorylation (Fig. 6i) in comparison to control littermates. These results suggest that the neonatal induction of intestinal *G6pc1* preserves adult hypothalamic leptin sensitivity after a nutritional challenge. We have previously shown that the induction of IGN in adult mice promotes P-STAT3 independently of leptin [32]. Moreover, P-STAT3/STAT3 levels correlate with G6Pase activity (Pearson=0.64, R^2=0.41, p=0.02) but not with leptin levels (Pearson=-0.31, R^2=0.10, p=0.33). Therefore, the observed increase in P-STAT3/STAT3 hypothalamic levels likely reflect IGN-derived signaling rather than leptin signaling. Importantly, adult I.G6pc$^{overexp\text{-}P1}$ mice still show an increase in intestinal *G6pc1* expression and G6Pase activity compared to littermates (Fig. 6j-k).

Overall, these data suggest that the neonatal induction of intestinal *G6pc1* protects against glucose intolerance, increased adiposity and hypothalamic leptin insensitivity in mice challenged with a hypercaloric diet during adulthood.

3.6 Inducing IGN after P12 fails to protect adult mice metabolism under a HFHS diet

To assess whether inducing intestinal *G6pc1* after its neonatal surge still affects adult metabolism, we challenged both I.G6pc$^{overexp\text{-}P12}$ and control mice with a HFHS diet since they were 6 weeks of age and for two months. In contrast to adult I.G6pc$^{overexp\text{-}P1}$ mice, adult I.G6pc$^{overexp\text{-}P12}$ mice display a body weight similar to controls (Fig. 7a). Moreover, in contrast to I.G6pc$^{overexp\text{-}P1}$ mice, I.G6pc$^{overexp\text{-}P12}$ mice were not protected from alterations in body fat accumulation (Fig. 7b), lean mass (Fig. 7c), energy expenditure (Fig. 7d), glucose intolerance (Fig. 7e), insulin resistance (Fig. 7f) or insulinemia (Fig. 7g) after being fed a HFHS diet. Furthermore, plasma leptin levels and hypothalamic STAT3 phosphorylation were equivalent in both I.G6pc$^{overexp\text{-}P12}$ and control mice (Fig. 7h-i), suggesting no protection against hypothalamic leptin resistance, as seen in I.G6pc$^{overexp\text{-}P1}$. Wild-type mice with a tamoxifen

administration at P12 did not exhibit any tamoxifen-induced effects on weight and body composition but they did exhibit mild glucose and insulin intolerance (Supplemental Fig. 7). Importantly, this suggests that the mild alteration in glucose tolerance observed in I.G6pc$^{overexp-P12}$ mice could be due to the injection of tamoxifen at P12 and not the induction of intestinal *G6pc1*. These results suggest that the protective effect of IGN against the detrimental metabolic and hypothalamic effects of a HFHS diet is restricted to the first two weeks of life. Of note, I.G6pc$^{overexp-P12}$ mice also showed an increase in intestinal G6Pase activity and *G6pc1* expression compared to littermates (Fig. 7j-k). Importantly, the expression of intestinal *G6pc1* and G6Pase activity of I.G6pc$^{overexp-P12}$ mice were not decreased in comparison to I.G6pc$^{overexp-P1}$ (Supplemental Fig. 8a-b).

3.7 The neonatal induction of IGN modulates adult mice adipose tissue

We recently demonstrated that the beneficial effects of the constitutive IGN activation on weight gain, energy expenditure and glucose tolerance were linked to adipose tissue plasticity. In agreement with these findings, the decreased body fat mass observed in adult I.G6pc$^{overexp-P1}$ mice was associated with an increased number of adipocytes per area in the subcutaneous inguinal (iWAT) and a trend to an increase in the number of adipocytes in the epididymal (epiWAT) adipose tissues (Fig. 8a-b), suggesting that I.G6pc$^{overexp-P1}$ mice have smaller adipocytes in these adipose tissues.

Our previous studies revealed that the anti-obesity effects of IGN activation were mediated by the stimulation of adipose tissue thermogenesis through the sympathetic nervous system (SNS) [35]. These findings raised the question of whether the diminution of inguinal and epididymal adipocyte size could be due to an increase in sympathetic tone. To test this hypothesis, we evaluated by western blots the expression of tyrosine hydroxylase (TH), a marker of sympathetic fibers, in the iWAT and epiWAT. In agreement with our morphological analyses of adipocyte size, TH protein levels were increased in the epiWAT of adult I.G6pc$^{overexp-P1}$ mice compared to their littermates (Fig. 8c-d), suggesting that the neonatal induction of intestinal *G6pc1* was associated with an increase in sympathetic innervation into this adipose tissue in adult mice under a HFHS diet. The neonatal induction of intestinal *G6pc1* was also associated with a tendency to an increase in TH protein and *Ucp1* mRNA levels in the brown adipose tissue (BAT) (Fig. 8e-f), also suggesting an increase in sympathetic innervation of the BAT in adult I.G6pc$^{overexp-P1}$ mice under a HFHS diet.

Similar to the lack of protection against glucose intolerance, leptin resistance and increased adiposity when fed a HFHS diet, I.G6pc$^{overexp-P12}$ mice also showed no increase in TH protein

levels of the iWAT, epiWAT or BAT, in contrast to what was observed in I.G6pc$^{overexp-P1}$ mice (Fig. 8g-i). These results suggest that the stimulating effect of intestinal *G6pc1* on epiWAT and BAT sympathetic innervation is also restricted to a neonatal critical period.

3.8 The constitutive induction of IGN stimulates adipose tissue sympathetic innervation during the neonatal period.

The sympathetic innervation of the white adipose tissues develops in the perinatal period, from birth to P21 [47], thereby controlling adipose tissue plasticity in the adulthood. We thus tested the hypothesis that IGN could modulate sympathetic fibers during the neonatal period. The amount of TH protein levels was similar between I.G6pc$^{overexp-P1}$ mouse pups at P20 and their control littermates, in the different white and brown adipose tissues studied (Fig. 8j-k). However, TH protein levels were increased in the BAT of I.G6pc$^{overexp-c}$ mouse pups at P15, but not in the iWAT or the epiWAT (Fig. 8l-n). These results suggest that the constitutive induction of intestinal *G6pc1* promotes BAT sympathetic innervation, but that this regulation did not take place in the inducible model at P1. Of note, intestinal *G6pc1* expression was similarly induced in I.G6pc$^{overexp-P1}$ and in I.G6pc$^{overexp-c}$ mouse pups at P15 when compared to controls (Supplemental Fig. 8c)**.**

4. Discussion

Intestinal gluconeogenesis controls a gut-brain neural circuit that is crucial for metabolic health [27,28]. This circuit is mobilized in adults under specific nutritional conditions, such as a diet rich in proteins [48] or in soluble fibers [49–51] or after gastric bypass surgery [52]. The metabolic benefits of IGN are mediated through hypothalamic STAT3 signaling, albeit independently of leptin [32] . Especially, IGN promotes BAT thermogenesis via the activation of the BAT sympathetic innervation [35]. Interestingly, similarly to leptin, there is a surge in IGN activity during the first two weeks of postnatal life [26]. However, the role of the neonatal IGN surge remained uncharacterized. Here, we show that during neonatal life, IGN complements the action of leptin by influencing the development of hypothalamic neuron circuits and of adipose tissue innervation, which contributes to the long-term regulation of energy balance in adulthood.

Malnutrition during gestation and lactation is known to affect the development of hypothalamic melanocortin circuits [6]. It should be noted that the neonatal context is an environment conducive to hypoglycaemia, because of the relative lack of glucose in milk [53]. To maintain

normoglycaemia, and thus survival, endogenous glucose production (EGP) is rapidly activated in the neonate, which is assured by glycogenolysis in the liver [54], and gluconeogenesis in the liver, kidney and intestine [26,53,55,56]. The expected role of IGN during neonatal life would therefore be to provide glucose for the growing neonate. However, our data indicate that glycaemia was unaltered in I.G6pc$^{overexp-P1}$ pups. In addition, plasma insulin levels were equivalent in both G6pc$^{overexp-P1}$ pups and control littermates. Moreover, several data suggest that neonatal EGP is mostly assured by the liver. In fact, rat fetuses stock large quantities of hepatic glycogen prior to birth, and the liver rapidly mobilizes these glycogen reserves during the early neonatal period to maintain blood sugar levels [54]. Accordingly, the activity of glucose-6-phosphatase, the mandatory enzyme of EGP, is more than 7-times higher in the liver than in the intestine of the newborn [26]. In addition, a neonatal diminution of hepatic gluconeogenesis is sufficient to produce hypoglycaemia in neonates [57], further highlighting the key role of the liver in the regulation of glycaemia in the neonate. Thus, maintaining glycaemia during the early postnatal period is probably not a major role of neonatal IGN. Instead, our results reveal that neonatal induction of intestinal *G6pc1* controls the development of AgRP and POMC neural projections to the PVHant. Because glycemia and insulinemia were normal in G6pc$^{overexp-P1}$ pups, this suggests that the neurodevelopmental effects observed in these mice were not a consequence of variations in plasma glucose or insulin levels.

Perinatal IGN probably controls neuronal fiber growth through a gut-brain axis. In adults, IGN signals the brain through a nervous signal initiated by glucose detection in the portal vein, which activates the parabrachial nucleus and the hypothalamus through a mechanisms depending on CGRP neurons [32]. The elements for this gut-brain neural circuit activated by IGN are already present during the early postnatal period: the portal vein innervation, the dorsal root ganglia, which harbour the cell bodies of visceral splanchnic afferents, and CGRP neurons [58–60]. This information suggests that the gut-brain axis triggered by IGN could already be functioning during the early postnatal period, and that the mechanism linking postnatal IGN to its developmental effect on the brain could be a postnatal portal glucose signal sent to the hypothalamus.

Alterations in plasma leptin levels in pups exposed to perinatal malnutrition has repeatedly been associated with an insufficient development of ARH projections to the PVHant [61–63]. In addition, leptin-deficient *ob/ob* mice and LepRb-deficient *db/db* mice exhibit a decrease in AgRP and POMC fibers projecting to the PVHant, illustrating that leptin exerts neurotrophic effects on both POMC and AgRP neurons [18,22]. Similarly to leptin, our results show that modulating neonatal intestinal *G6pc1* controls the development of the melanocortin system.

Neonatal induction of intestinal *G6pc1*, either constitutively or at P1, leads to a transitional reorganization of AgRP and POMC fiber connections to the PVHant. The induction of intestinal *G6pc1* just after birth causes an increase in AgRP fibers and a reduction in POMC fibers connecting the PVHant, whereas the constitutive induction of intestinal *G6pc1* leads to a decrease in POMC fibers only. Our results suggest that despite the fact that both leptin and IGN are endogenously induced during the first two weeks of life, they would exert opposing action on the development of POMC fibers but a similar effect on AgRP fibers connecting the PVHant. Thus, the differential effects of leptin and IGN on POMC fibers may reflect complementarity in the mechanisms regulating the development of the neonatal melanocortin system. This complementarity may be a key factor in the optimal regulation of energy homeostasis in adults. Previous studies showed that leptin and particularly the STAT3 signaling pathway induced by the activation of the leptin receptor LepRb are critical factors involved in the development of POMC and AgRP neurite outgrowth during the perinatal period. Mimicking IGN in adult mice increases STAT3 phosphorylation in POMC neurons and in POMC-negative cells localized in the vicinity [32], raising the possibility that IGN increases STAT3 phosphorylation also in AgRP neurons. Our results suggest that the induction of intestinal *G6pc1* also promotes STAT3 phosphorylation in the hypothalamus of pups through a leptin-independent signaling pathway and/or enhanced leptin sensitivity. Consequently, neonatal induction of intestinal *G6pc1* might control ARH projections to the PVHant by controlling STAT3 phosphorylation in ARH, including POMC and AgRP neurons. However, since STAT3 phosphorylation was assessed at the whole hypothalamus level by western-blot and in ARH by immunofluorescence, we cannot exclude the possibility that the reduced leptin levels measured in P9 G6pc$^{overexp\text{-}P1}$ pups may lead to a decrease in LepRb-mediated STAT3 phosphorylation specifically in POMC and/or AgRP neurons. This reduction may be masked by an increase in other cell populations and/or hypothalamic nuclei. LepRb-mediated STAT3 phosphorylation is essential for the development of ARH POMC neurons but can be compensated by other signaling pathways in AgRP projections [22]. Therefore, a decrease in LepRb-mediated P-STAT3 in POMC neurons could explain the specific reduction in POMC fiber density observed in the PVH of G6pc$^{overexp\text{-}P1}$ and G6pc$^{overexp\text{-}c}$ pups.

We previously demonstrated in adult mice that IGN promotes hypothalamic STAT3 phosphorylation independently of leptin, through a gut-brain circuitry involving the calcitonin gene-related peptide (CGRP) [32]. Moreover, the IGN-induced STAT3 phosphorylation might be mediated by a direct effect of CGRP on ARH neurons [32]. The CGRP receptor is associated with RAMP1 and coupled to adenylyl cyclase via the G-proteins αs, αi and αq [64–66].

Interestingly, the stimulation of Gαs or the direct activation of adenylyl cyclase both promote STAT3 phosphorylation [65], while RAMP1/3-deficient mice exhibit decreased AgRP- and POMC-derived α-MSH fiber densities in the PVHant [67]. Future experiments will be needed to investigate whether IGN promotes AgRP axonal development via CGRP and a CGRP receptor-mediated STAT3 phosphorylation.

Importantly, our results demonstrated that the transitional changes in the POMC/AgRP fiber density induced by the neonatal induction of intestinal *G6pc1* have lasting beneficial effects on adult hypothalamic functions and whole-body metabolism.

We recently demonstrated that a constitutive activation of IGN promotes metabolic benefits by involving thermogenesis and the BAT sympathetic innervation. Sympathetic innervation of white and brown adipose tissues emerges between P6-P10 and reaches the adult innervation pattern around P21-P28 [68,69]. The sympathetic innervation of fat cells in this early neonatal period is crucial for the maintenance of adipose tissue innervation in adulthood [69]. Moreover, POMC and AgRP neurons projecting to the PVH control sympathetic WAT and BAT innervations through hypothalamic STAT3 signalling [24]. Our results show that the neonatal induction of intestinal *G6pc1* promotes projections of AgRP neurons specifically to the PVH, hypothalamic STAT3 phosphorylation, adult epiWAT and BAT innervation and metabolic benefits, while the induction of intestinal *G6pc1* after P12 fails to produce comparable benefits. Based on our findings and previous observations described above, it is therefore possible that neonatal IGN might control adipose tissue innervation by promoting optimal projections of AgRP to the PVH, thereby contributing to the lower susceptibility of adult mice to develop metabolic defects under a hypercaloric diet.

A fascinating issue relates to the putative mechanisms capable of triggering the physiological induction of IGN in the neonatal period. In adulthood, IGN is stimulated under the action of specific macronutrients, such as protein or soluble fiber [31,49,50]. Indeed, both nutrient types induce intestinal gluconeogenic gene expression, via peptides for protein and via short-chain fatty acids (SCFA) for fiber, after its microbial fermentation. In addition, they also provide gluconeogenic substrates to IGN, i.e. glutamine and glutamate for protein and propionate and succinate for fiber [70,71]. It is noteworthy that milk is rich in protein and various complex carbohydrates with fiber properties [72,73]. Moreover, caseins that are major milk proteins are composed of glutamine/glutamate at a level of 20 % of their amino acids. The milk supply by

the mother in nutrients able to activate IGN might thus be a key lever to stimulate perinatal IGN in the pups.

It is noteworthy that the importance of the maternal microbiota in the metabolic programming of the offspring (and more specifically the microbial capacity to produce SCFA) was recently highlighted [74]. Promoting SCFA production in the pregnant mother might thus contribute to induce perinatal IGN in the offspring and the beneficial effects that we describe in this work. Consistent with this hypothesis, increasing SCFA-related bacteria in the offspring (by maternal exercise) promotes IGN and protects against the metabolic defects induced by a hypercaloric diet [75]. Interestingly, in line with our results, these protective effects are linked with an induction of BAT thermogenesis [76]. It is also worth mentioning here that human breast milk itself contains various oligosaccharides that are considered essential for the establishment of the baby's gut microbiota during the neonatal period [72,73]. Consistently, breastfeeding is associated with enhanced intestinal gluconeogenesis in infants [77]. Since the composition of breast milk depends on diet [78], this opens up a new prospect of modifying the composition of the maternal diet to promote neonatal IGN and metabolic health [79–81].

In conclusion, our results have highlighted that the neonatal induction of intestinal *G6pc1*, specifically during the first two weeks of postnatal life modulates the density of AgRP/POMC projections to the PVHant and promotes the sympathetic innervation of the BAT and epiWAT. Thus, the induction of intestinal *G6pc1* per *se* during the early neonatal period enables an optimal maturation of the hypothalamus and protects the metabolism of adult mice exposed to a metabolic challenge. Our study provides further evidence for the physiological importance of IGN in metabolic health through the dialogue it establishes with the brain, and opens up prospects for developing its protective role in adverse perinatal environments.

Abbreviations:

IGN, intestinal gluconeogenesis; AgRP: agouti-related peptide; POMC: pro-opiomelanocortin; ARH: arcuate nucleus; PVHant: paraventricular nucleus anterior; PVHpost: paraventricular nucleus posterior; DMH: dorsomedial nucleus; LH: lateral hypothalamic area; 3V: 3rd ventricle; STAT3: transcription factor signal transducer and activator of transcription 3; CGRP: calcitonin gene-related peptide; HF/HS, high-fat/high-sucrose, BAT: brown adipose tissue; TH: tyrosine hydroxylase.

Acknowledgments

The authors acknowledge the SFR Lyon Est (CNRS UMS3453 - INSERM US7, UCBL1) facilities and particularly thank the members of the "Animalerie Lyon Est Conventionnelle et SPF" for animal care, the members of the CIQLE platform for confocal imaging and the members of the ANIPHY platform (Valerie Oréa and Delphine Guyonnet) for assessing body composition and calorimetry experiments.

Credit Authorship Contribution Statement

Judith Estrada-Meza : Writing – review & editing, Writing – original draft, Methodology, Investigation, Formal analysis, Data curation, Conceptualization. **Jasmine Videlo** : Investigation, Formal analysis. **Clara Bron** : Investigation. **Adeline Duchampt** : Investigation, Formal analysis. **Cécile Saint-Béat** : Investigation. **Mickael Zergane** : Investigation, Formal analysis. **Marine Silva** : Investigation. **Fabienne Rajas** : Resources. **Sebastien G. Bouret** : Writing – review & editing, Methodology, Funding acquisition. **Gilles Mithieux**: Writing – review & editing, Resources, Conceptualization, Funding acquisition. **Amandine Gautier-Stein**: Writing – review & editing, Methodology, Formal analysis, Data curation, Conceptualization, Funding acquisition, Supervision, Project administration.

Funding

The work was funded by the Institut Benjamin Delessert, the Société Francophone du Diabète and the European Research Council (project IGN-101097330), and the Agence Nationale pour la Recherche (project MATBIOTA ANR-22-CE-16-0007).

Declaration of competing interest

The authors declare no competing interests.

Data availability

Further information and requests for resources and reagents should be directed to and will be fulfilled by Amandine Gautier-Stein (amandine.gautier-stein@univ-lyon1.fr).

References:

[1] Ebbeling, C.B., Pawlak, D.B., Ludwig, D.S., 2002. Childhood obesity: public-health crisis, common sense cure. Lancet (London, England) 360(9331): 473–82, Doi: 10.1016/S0140-6736(02)09678-2.

[2] Saklayen, M.G., 2018. The Global Epidemic of the Metabolic Syndrome. Current Hypertension Reports 20(2): 12, Doi: 10.1007/s11906-018-0812-z.

[3] Cottrell, E.C., Ozanne, S.E., 2007. Developmental programming of energy balance and the metabolic syndrome. Proceedings of the Nutrition Society 66(2): 198–206, Doi: 10.1017/S0029665107005447.

[4] Moullé, V.S., Parnet, P., 2019. Effects of Nutrient Intake during Pregnancy and Lactation on the Endocrine Pancreas of the Offspring. Nutrients 11(11): 2708, Doi: 10.3390/nu11112708.

[5] Bouret, S.G., 2022. Developmental programming of hypothalamic melanocortin circuits. Experimental & Molecular Medicine 54(4): 403–13, Doi: 10.1038/s12276-021-00625-8.

[6] Coupé, B., Amarger, V., Grit, I., Benani, A., Parnet, P., 2010. Nutritional programming affects hypothalamic organization and early response to leptin. Endocrinology 151(2): 702–13, Doi: 10.1210/en.2009-0893.

[7] Park, S., Belfoul, A.M., Rastelli, M., Jang, A., Monnoye, M., Bae, H., et al., 2023. Maternal low-calorie sweetener consumption rewires hypothalamic melanocortin circuits via a gut microbial co-metabolite pathway. JCI Insight 8(10): e156397, Doi: 10.1172/jci.insight.156397.

[8] Steculorum, S.M., Collden, G., Coupe, B., Croizier, S., Lockie, S., Andrews, Z.B., et al., 2015. Neonatal ghrelin programs development of hypothalamic feeding circuits. Journal of Clinical Investigation 125(2): 846–58, Doi: 10.1172/JCI73688.

[9] Sullivan, E.L., Rivera, H.M., True, C.A., Franco, J.G., Baquero, K., Dean, T.A., et al., 2017. Maternal and postnatal high-fat diet consumption programs energy balance and hypothalamic melanocortin signaling in nonhuman primate offspring. American Journal of Physiology. Regulatory, Integrative and Comparative Physiology 313(2): R169–79, Doi: 10.1152/ajpregu.00309.2016.

[10] Cone, R.D., 2005. Anatomy and regulation of the central melanocortin system. Nature Neuroscience 8(5): 571–8, Doi: 10.1038/nn1455.

[11] Wu, Q., Palmiter, R.D., 2011. GABAergic signaling by AgRP neurons prevents anorexia via a melanocortin-independent mechanism. European Journal of Pharmacology 660(1): 21–7, Doi: 10.1016/j.ejphar.2010.10.110.

[12] Wu, Q., Boyle, M.P., Palmiter, R.D., 2009. Loss of GABAergic signaling by AgRP neurons to the parabrachial nucleus leads to starvation. Cell 137(7): 1225–34, Doi: 10.1016/j.cell.2009.04.022.

[13] Berthoud, H.-R., 2002. Multiple neural systems controlling food intake and body weight. Neuroscience & Biobehavioral Reviews 26(4): 393–428.

[14] Levin, B.E., 2000. The Obesity Epidemic: Metabolic Imprinting on Genetically Susceptible Neural Circuits. Obesity Research 8(4): 342–7, Doi: 10.1038/oby.2000.41.

[15] Bouret, S.G., 2017. Development of Hypothalamic Circuits That Control Food Intake and Energy Balance. In: Harris, R.B.S., editor. Appetite and Food Intake, 2nd ed. Second edition. | Boca Raton : CRC Press, 2017. | Previous edition: CRC Press p. 135–54.

[16] Colldén, G., Caron, E., Bouret, S.G., 2022. Neonatal leptin antagonism improves metabolic programming of postnatally overnourished mice. International Journal of Obesity (2005) 46(6): 1138–44, Doi: 10.1038/s41366-022-01093-4.

[17] Bouret, S.G., 2004. Formation of Projection Pathways from the Arcuate Nucleus of the Hypothalamus to Hypothalamic Regions Implicated in the Neural Control of Feeding

Behavior in Mice. Journal of Neuroscience 24(11): 2797–805, Doi: 10.1523/JNEUROSCI.5369-03.2004.
[18] Bouret, S.G., 2004. Trophic Action of Leptin on Hypothalamic Neurons That Regulate Feeding. Science 304(5667): 108–10, Doi: 10.1126/science.1095004.
[19] Bouret, S.G., 2013. Organizational actions of metabolic hormones. Frontiers in Neuroendocrinology 34(1): 18–26, Doi: 10.1016/j.yfrne.2013.01.001.
[20] Ahima, R.S., Prabakaran, D., Flier, J.S., 1998. Postnatal leptin surge and regulation of circadian rhythm of leptin by feeding. Implications for energy homeostasis and neuroendocrine function. Journal of Clinical Investigation 101(5): 1020.
[21] Devaskar, S.U., Ollesch, C., Rajakumar, R.A., Rajakumar, P.A., 1997. Developmental changes in ob gene expression and circulating leptin peptide concentrations. Biochemical and Biophysical Research Communications 238(1): 44–7, Doi: 10.1006/bbrc.1997.7237.
[22] Bouret, S.G., Bates, S.H., Chen, S., Myers, M.G., Simerly, R.B., 2012. Distinct Roles for Specific Leptin Receptor Signals in the Development of Hypothalamic Feeding Circuits. Journal of Neuroscience 32(4): 1244–52, Doi: 10.1523/JNEUROSCI.2277-11.2012.
[23] Croizier, S., Prevot, V., Bouret, S.G., 2016. Leptin controls parasympathetic wiring of the pancreas during embryonic life. Cell Reports 15(1): 36–44, Doi: 10.1016/j.celrep.2016.02.088.
[24] Wang, P., Loh, K.H., Wu, M., Morgan, D.A., Schneeberger, M., Yu, X., et al., 2020. A leptin-BDNF pathway regulating sympathetic innervation of adipose tissue. Nature 583(7818): 839–44, Doi: 10.1038/s41586-020-2527-y.
[25] Wu, R., Yu, W., Fu, L., Li, F., Jing, J., Cui, X., et al., 2020. Postnatal leptin surge is critical for the transient induction of the developmental beige adipocytes in mice. American Journal of Physiology. Endocrinology and Metabolism 318(4): E453–61, Doi: 10.1152/ajpendo.00292.2019.
[26] Chatelain, F., Pégorier, J.P., Minassian, C., Bruni, N., Tarpin, S., Girard, J., et al., 1998. Development and regulation of glucose-6-phosphatase gene expression in rat liver, intestine, and kidney: in vivo and in vitro studies in cultured fetal hepatocytes. Diabetes 47(6): 882–9.
[27] Soty, M., Penhoat, A., Amigo-Correig, M., Vinera, J., Sardella, A., Vullin-Bouilloux, F., et al., 2015. A gut–brain neural circuit controlled by intestinal gluconeogenesis is crucial in metabolic health. Molecular Metabolism 4(2): 106–17, Doi: 10.1016/j.molmet.2014.12.009.
[28] Vily-Petit, J., Soty-Roca, M., Silva, M., Raffin, M., Gautier-Stein, A., Rajas, F., et al., 2020. Intestinal gluconeogenesis prevents obesity-linked liver steatosis and non-alcoholic fatty liver disease. Gut, Doi: 10.1136/gutjnl-2019-319745.
[29] Delaere, F., Akaoka, H., De Vadder, F., Duchampt, A., Mithieux, G., 2013. Portal glucose influences the sensory, cortical and reward systems in rats. European Journal of Neuroscience 38(10): 3476–86, Doi: 10.1111/ejn.12354.
[30] Delaere, F., Magnan, C., Mithieux, G., 2010. Hypothalamic integration of portal glucose signals and control of food intake and insulin sensitivity. Diabetes & Metabolism 36(4): 257–62, Doi: 10.1016/j.diabet.2010.05.001.
[31] Mithieux, G., Misery, P., Magnan, C., Pillot, B., Gautier-Stein, A., Bernard, C., et al., 2005. Portal sensing of intestinal gluconeogenesis is a mechanistic link in the diminution of food intake induced by diet protein. Cell Metabolism 2(5): 321–9, Doi: 10.1016/j.cmet.2005.09.010.
[32] Soty, M., Vily-Petit, J., Castellanos-Jankiewicz, A., Guzman-Quevedo, O., Raffin, M., Clark, S., et al., 2021. Calcitonin Gene-Related Peptide-Induced Phosphorylation of

STAT3 in Arcuate Neurons Is a Link in the Metabolic Benefits of Portal Glucose. Neuroendocrinology 111(6): 555–67, Doi: 10.1159/000509230.
[33] Lizen, B., Claus, M., Jeannotte, L., Rijli, F.M., Gofflot, F., 2015. Perinatal induction of Cre recombination with tamoxifen. Transgenic Research 24(6): 1065–77, Doi: 10.1007/s11248-015-9905-5.
[34] Abdul-Wahed, A., Gautier-Stein, A., Casteras, S., Soty, M., Roussel, D., Romestaing, C., et al., 2014. A link between hepatic glucose production and peripheral energy metabolism via hepatokines. Molecular Metabolism 3(5): 531–43, Doi: 10.1016/j.molmet.2014.05.005.
[35] Vily-Petit, J., Soty-Roca, M., Silva, M., Micoud, M., Evrard, F., Bron, C., et al., 2024. Anti-obesity effects of intestinal gluconeogenesis are mediated by the brown adipose tissue sympathetic nervous system. Obesity (Silver Spring): 1–13, Doi: 10.1002/oby.23985.
[36] Mina, A.I., LeClair, R.A., LeClair, K.B., Cohen, D.E., Lantier, L., Banks, A.S., 2018. CalR: A Web-Based Analysis Tool for Indirect Calorimetry Experiments. Cell Metabolism 28(4): 656-666.e1, Doi: 10.1016/j.cmet.2018.06.019.
[37] Metzger, D., Chambon, P., 2001. Site- and Time-Specific Gene Targeting in the Mouse. Methods 24(1): 71–80, Doi: 10.1006/meth.2001.1159.
[38] Ichimura, R., Takahashi, M., Morikawa, T., Inoue, K., Kuwata, K., Usuda, K., et al., 2016. Neonatal exposure to SERMs disrupts neuroendocrine development and postnatal reproductive function through alteration of hypothalamic kisspeptin neurons in female rats. Neurotoxicology 56: 64–75, Doi: 10.1016/j.neuro.2016.07.003.
[39] Agça, E., Batailler, M., Tillet, Y., Chemineau, P., Duittoz, A.H., 2008. Modulation of estrogen receptors during development inhibits neurogenesis of precursors to GnRH-1 neurones: in vitro studies with explants of ovine olfactory placode. Brain Research 1223: 34–41, Doi: 10.1016/j.brainres.2008.05.026.
[40] van der Klaauw, A.A., Croizier, S., Mendes de Oliveira, E., Stadler, L.K.J., Park, S., Kong, Y., et al., 2019. Human Semaphorin 3 Variants Link Melanocortin Circuit Development and Energy Balance. Cell 176(4): 729-742.e18, Doi: 10.1016/j.cell.2018.12.009.
[41] Rozo, A.V., Babu, D.A., Suen, P.A., Groff, D.N., Seeley, R.J., Simmons, R.A., et al., 2017. Neonatal GLP1R activation limits adult adiposity by durably altering hypothalamic architecture. Molecular Metabolism 6(7): 748–59, Doi: 10.1016/j.molmet.2017.05.006.
[42] Estrada-Meza, J., Videlo, J., Bron, C., Saint-Béat, C., Silva, M., Duboeuf, F., et al., 2021. Tamoxifen Treatment in the Neonatal Period Affects Glucose Homeostasis in Adult Mice in a Sex-Dependent Manner. Endocrinology 162(7): bqab098, Doi: 10.1210/endocr/bqab098.
[43] Bouhajja, H., Bougacha-Elleuch, N., Lucas, N., Legrand, R., Marrakchi, R., Kaveri, S.V., et al., 2018. Affinity kinetics of leptin-reactive immunoglobulins are associated with plasma leptin and markers of obesity and diabetes. Nutrition & Diabetes 8(1): 32, Doi: 10.1038/s41387-018-0044-y.
[44] Kettaneh, A., Heude, B., Romon, M., Oppert, J.M., Borys, J.M., Balkau, B., et al., 2007. High plasma leptin predicts an increase in subcutaneous adiposity in children and adults. European Journal of Clinical Nutrition 61(6): 719–26, Doi: 10.1038/sj.ejcn.1602579.
[45] Izquierdo, A.G., Crujeiras, A.B., Casanueva, F.F., Carreira, M.C., 2019. Leptin, Obesity, and Leptin Resistance: Where Are We 25 Years Later? Nutrients 11(11): 2704, Doi: 10.3390/nu11112704.

[46] Jung, C.H., Kim, M.-S., 2013. Molecular mechanisms of central leptin resistance in obesity. Archives of Pharmacal Research 36(2): 201–7, Doi: 10.1007/s12272-013-0020-y.
[47] Chabowska-Kita, A., Kozak, L.P., 2016. The critical period for brown adipocyte development: Genetic and environmental influences. Obesity (Silver Spring, Md.) 24(2): 283–90, Doi: 10.1002/oby.21376.
[48] Duraffourd, C., De Vadder, F., Goncalves, D., Delaere, F., Penhoat, A., Brusset, B., et al., 2012. Mu-opioid receptors and dietary protein stimulate a gut-brain neural circuitry limiting food intake. Cell 150(2): 377–88.
[49] De Vadder, F., Kovatcheva-Datchary, P., Goncalves, D., Vinera, J., Zitoun, C., Duchampt, A., et al., 2014. Microbiota-generated metabolites promote metabolic benefits via gut-brain neural circuits. Cell 156(1–2): 84–96, Doi: 10.1016/j.cell.2013.12.016.
[50] De Vadder, F., Kovatcheva-Datchary, P., Zitoun, C., Duchampt, A., Bäckhed, F., Mithieux, G., 2016. Microbiota-Produced Succinate Improves Glucose Homeostasis via Intestinal Gluconeogenesis. Cell Metabolism 24(1): 151–7, Doi: 10.1016/j.cmet.2016.06.013.
[51] Sinet, F., Soty, M., Zemdegs, J., Guiard, B., Estrada, J., Malleret, G., et al., 2021. Dietary Fibers and Proteins Modulate Behavior via the Activation of Intestinal Gluconeogenesis. Neuroendocrinology, Doi: 10.1159/000514289.
[52] Troy, S., Soty, M., Ribeiro, L., Laval, L., Migrenne, S., Fioramonti, X., et al., 2008. Intestinal gluconeogenesis is a key factor for early metabolic changes after gastric bypass but not after gastric lap-band in mice. Cell Metab 8(3): 201–11.
[53] Girard, J., Ferré, P., Pégorier, J.P., Duée, P.H., 1992. Adaptations of glucose and fatty acid metabolism during perinatal period and suckling-weaning transition. Physiological Reviews 72(2): 507–62, Doi: 10.1152/physrev.1992.72.2.507.
[54] Margolis, R.N., Tanner, K., 1986. Glycogen metabolism in neonatal liver of the rat. Archives of Biochemistry and Biophysics 249(2): 605–10, Doi: 10.1016/0003-9861(86)90039-1.
[55] Hahn, P., Taller, M., Chan, H., 1988. Pyruvate carboxylase, phosphate-dependent glutaminase and glutamate dehydrogenase in the developing rat small intestinal mucosa. Biology of the Neonate 53(6): 362–6, Doi: 10.1159/000242814.
[56] Watford, M., Tatro, A.V., 1989. Phosphoenolpyruvate carboxykinase of rat small intestine: distribution and regulation of activity and mRNA levels. The Journal of Nutrition 119(2): 268–72, Doi: 10.1093/jn/119.2.268.
[57] Cotter, D.G., Ercal, B., André d'Avignon, D., Dietzen, D.J., Crawford, P.A., 2014. Impairments of hepatic gluconeogenesis and ketogenesis in PPARα-deficient neonatal mice. American Journal of Physiology-Endocrinology and Metabolism 307(2): E176–85, Doi: 10.1152/ajpendo.00087.2014.
[58] Crawford, L.W., Foley, J.F., Elmore, S.A., 2010. Histology Atlas of the Developing Mouse Hepatobiliary System with Emphasis on Embryonic Days 9.5-18.5. Toxicologic Pathology 38(6): 872–906, Doi: 10.1177/0192623310374329.
[59] Ody, M., Thiévent, A., Millet, M., Connat, J.-L., 1993. Postnatal development of the rat portal vein: correlation with occurrence of peptidergic innervation. Cell and Tissue Research 272(2): 303–14, Doi: 10.1007/BF00302735.
[60] Ozaki, S., Snider, W.D., 1997. Initial trajectories of sensory axons toward laminar targets in the developing mouse spinal cord. The Journal of Comparative Neurology 380(2): 215–29.

[61] Yura, S., Itoh, H., Sagawa, N., Yamamoto, H., Masuzaki, H., Nakao, K., et al., 2005. Role of premature leptin surge in obesity resulting from intrauterine undernutrition. Cell Metabolism 1(6): 371–8, Doi: 10.1016/j.cmet.2005.05.005.
[62] Delahaye, F., Breton, C., Risold, P.-Y., Enache, M., Dutriez-Casteloot, I., Laborie, C., et al., 2008. Maternal Perinatal Undernutrition Drastically Reduces Postnatal Leptin Surge and Affects the Development of Arcuate Nucleus Proopiomelanocortin Neurons in Neonatal Male Rat Pups. Endocrinology 149(2): 470–5, Doi: 10.1210/en.2007-1263.
[63] Kirk, S.L., Samuelsson, A.-M., Argenton, M., Dhonye, H., Kalamatianos, T., Poston, L., et al., 2009. Maternal Obesity Induced by Diet in Rats Permanently Influences Central Processes Regulating Food Intake in Offspring. PLoS ONE 4(6): e5870, Doi: 10.1371/journal.pone.0005870.
[64] Kumar, A., Potts, J.D., DiPette, D.J., 2019. Protective Role of α-Calcitonin Gene-Related Peptide in Cardiovascular Diseases. Frontiers in Physiology 10: 821, Doi: 10.3389/fphys.2019.00821.
[65] Liu, A.M.F., Lo, R.K.H., Wong, C.S.S., Morris, C., Wise, H., Wong, Y.H., 2006. Activation of STAT3 by G alpha(s) distinctively requires protein kinase A, JNK, and phosphatidylinositol 3-kinase. The Journal of Biological Chemistry 281(47): 35812–25, Doi: 10.1074/jbc.M605288200.
[66] Weston, C., Winfield, I., Harris, M., Hodgson, R., Shah, A., Dowell, S.J., et al., 2016. Receptor Activity-modifying Protein-directed G Protein Signaling Specificity for the Calcitonin Gene-related Peptide Family of Receptors. The Journal of Biological Chemistry 291(42): 21925–44, Doi: 10.1074/jbc.M116.751362.
[67] Lutz, T.A., Coester, B., Whiting, L., Dunn-Meynell, A.A., Boyle, C.N., Bouret, S.G., et al., 2018. Amylin Selectively Signals Onto POMC Neurons in the Arcuate Nucleus of the Hypothalamus. Diabetes 67(5): 805–17, Doi: 10.2337/db17-1347.
[68] Berry, D.M., Daniel, H., 1970. Sympathetic nerve development in the brown adipose tissue of the rat. Canadian Journal of Physiology and Pharmacology 48(3): 160–8, Doi: https://doi.org/10.1139/y70-028.
[69] Chi, J., Lin, Z., Barr, W., Crane, A., Zhu, X.G., Cohen, P., 2021. Early postnatal interactions between beige adipocytes and sympathetic neurites regulate innervation of subcutaneous fat. ELife 10: e64693, Doi: 10.7554/eLife.64693.
[70] Gautier-Stein, A., Mithieux, G., 2023. Intestinal gluconeogenesis: metabolic benefits make sense in the light of evolution. Nature Reviews. Gastroenterology & Hepatology 20(3): 183–94, Doi: 10.1038/s41575-022-00707-6.
[71] Soty, M., Gautier-Stein, A., Rajas, F., Mithieux, G., 2017. Gut-Brain Glucose Signaling in Energy Homeostasis. Cell Metabolism 25(6): 1231–42, Doi: 10.1016/j.cmet.2017.04.032.
[72] Çavdar, G., Papich, T., Ryan, E.P., 2019. Microbiome, Breastfeeding and Public Health Policy in the United States: The Case for Dietary Fiber. Nutrition and Metabolic Insights 12: 1178638819869597, Doi: 10.1177/1178638819869597.
[73] Kim, S.Y., Yi, D.Y., 2020. Components of human breast milk: from macronutrient to microbiome and microRNA. Clinical and Experimental Pediatrics 63(8): 301–9, Doi: 10.3345/cep.2020.00059.
[74] Kimura, I., Miyamoto, J., Ohue-Kitano, R., Watanabe, K., Yamada, T., Onuki, M., et al., 2020. Maternal gut microbiota in pregnancy influences offspring metabolic phenotype in mice. Science (New York, N.Y.) 367(6481): eaaw8429, Doi: 10.1126/science.aaw8429.
[75] Zhang, L., Zou, W., Hu, Y., Wu, H., Gao, Y., Zhang, J., et al., 2023. Maternal voluntary wheel running modulates glucose homeostasis, the gut microbiota and its derived fecal metabolites in offspring. Clinical Science (London, England: 1979) 137(15): 1151–66, Doi: 10.1042/CS20230372.

[76] Son, J.S., Zhao, L., Chen, Y., Chen, K., Chae, S.A., de Avila, J.M., et al., 2020. Maternal exercise via exerkine apelin enhances brown adipogenesis and prevents metabolic dysfunction in offspring mice. Science Advances 6(16): eaaz0359, Doi: 10.1126/sciadv.aaz0359.
[77] Ni, D., Tan, J., Macia, L., Nanan, R., 2024. Breastfeeding is associated with enhanced intestinal gluconeogenesis in infants. BMC Medicine 22(1): 106, Doi: 10.1186/s12916-024-03327-w.
[78] Martin Agnoux, A., Antignac, J.-P., Boquien, C.-Y., David, A., Desnots, E., Ferchaud-Roucher, V., et al., 2015. Perinatal protein restriction affects milk free amino acid and fatty acid profile in lactating rats: potential role on pup growth and metabolic status. The Journal of Nutritional Biochemistry 26(7): 784–95, Doi: 10.1016/j.jnutbio.2015.02.012.
[79] Le Bourgot, C., Ferret-Bernard, S., Le Normand, L., Savary, G., Menendez-Aparicio, E., Blat, S., et al., 2014. Maternal short-chain fructooligosaccharide supplementation influences intestinal immune system maturation in piglets. PloS One 9(9): e107508, Doi: 10.1371/journal.pone.0107508.
[80] Le Bourgot, C., Le Normand, L., Formal, M., Respondek, F., Blat, S., Apper, E., et al., 2017. Maternal short-chain fructo-oligosaccharide supplementation increases intestinal cytokine secretion, goblet cell number, butyrate concentration and Lawsonia intracellularis humoral vaccine response in weaned pigs. The British Journal of Nutrition 117(1): 83–92, Doi: 10.1017/S0007114516004268.
[81] Oozeer, R., van Limpt, K., Ludwig, T., Ben Amor, K., Martin, R., Wind, R.D., et al., 2013. Intestinal microbiology in early life: specific prebiotics can have similar functionalities as human-milk oligosaccharides. The American Journal of Clinical Nutrition 98(2): 561S-71S, Doi: 10.3945/ajcn.112.038893.

Figure legends

Figure 1. Neonatal induction of intestinal gluconeogenesis. (**a**) Intestinal expression of *G6pc1* (coding for the catalytic unit of the glucose-6-phosphatase) during the first two weeks of life in mouse (mean ± SEM; n= 6-4 per age; significant differences from P5 values are indicated as ****:p<0.0001, One-way ANOVA followed by Tukey's post hoc test). (**b**) Schematic representation of the CRE-lox strategy leading to the intestine-specific inducible induction of *G6pc1*. ERT2: human estrogen receptor mutated to specifically bind 4-hydroxytamoxifen; LBD: ligand binding domain. (**c**) Intestinal specificity of the genetic modification in Control and I.G6pc$^{overexp\text{-}P1}$ mice aged of 15 days, and persistence of the genetic modification in I I.G6pc$^{overexp\text{-}P1}$ mice aged of 80 days. PCR genotype analysis based on intestinal genomic DNA, using the p1 and p2 primers (grey), yields products of 480 bp when the STOP cassette is excised. C= Control; I: I.G6pc$^{overexp\text{-}P1}$ (**d**) Induction of intestinal *G6pc1* expression in I.G6pc$^{overexp\text{-}P1}$ pups (white squares) compared to the one in Control pups (black squares) during the neonatal period. (mean ± SEM; n= 3-8 per age; significant differences from Control values are indicated as *:p<0.05, multiple unpaired t-tests) (**e**) Intestinal G6Pase activity in Control (black squares) and I.G6pc$^{overexp\text{-}P1}$ pups (white squares) during the neonatal

period, expressed as fold over P1 values for each genotype (mean ± SEM; n= 3-14 per age; Two-way ANOVA followed by Sidak's post hoc test were performed as analyses. §:p<0.05 : differences from Control P1 values; **:p<0.01 and ***:p<0.001: differences from I.G6pc$^{overexp-P1}$ P1 values. $: p<0.05 and numbers: differences between Control and I.G6pc$^{overexp-P1}$ values at each age).

Figure 2. Neonatal induction of intestinal *G6pc1* influences the development of AgRP and POMC neural projections. (**a**) Schematic representation of hypothalamic nuclei that were quantified (with their corresponding bregma). Representative confocal images and quantification of (**b**) AgRP-immunoreactive and (**c**) POMC-immunoreactive fibers in P20 I.G6pc$^{overexp-P1}$ (white squares) and control littermates (black squares) (mean ± SEM; n= 5-6). Scale bar = 100µm. 3V: 3rd ventricle; PVHant: anterior part of the paraventricular nucleus; PVHpost: posterior part of the paraventricular nucleus; LH: lateral hypothalamic area; DMH: dorsomedial nucleus. Two-way ANOVA, followed by multiple comparisons and Sidak's post-hoc test were performed as statistical analyses. *p<0.05; **p<0.01.

Figure 3. Constitutive induction of intestinal *G6pc1* influences the development of POMC neural projections. (**a**) Schematic representation of hypothalamic nuclei that were quantified (with their corresponding bregma). Representative confocal images and quantification of (**b**) AgRP-immunoreactive and (**c**) POMC-immunoreactive fibers in P20 I.G6pc$^{overexp-c}$ (white squares) and control littermates (black squares) (mean ± SEM; n= 4-6). Scale bar = 100µm. 3V: 3rd ventricle; PVHant: anterior part of the paraventricular nucleus; PVHpost: posterior part of the paraventricular nucleus; LH: lateral hypothalamic area; DMH: dorsomedial nucleus. Two-way ANOVA, followed by multiple comparisons and Sidak's post-hoc test were performed as statistical analyses. **p<0.01.

Figure 4. Induction of intestinal *G6pc1* at P12 fails to influence the development of AgRP and POMC neural projections. (**a**) Schematic representation of hypothalamic nuclei that were quantified (with their corresponding bregma). Representative confocal images and quantification of (**b**) AgRP-immunoreactive and (**c**) POMC-immunoreactive fibers in P20 I.G6pc$^{overexp-P12}$ (white lozenges) and control littermates (black lozenges) (mean ± SEM; n= 5-6). Scale bar = 100µm. 3V: 3rd ventricle; PVHant: anterior part of the paraventricular nucleus; PVHpost: posterior part of the paraventricular nucleus; LH: lateral hypothalamic area; DMH:

dorsomedial nucleus. Two-way ANOVA, followed by multiple comparisons and Sidak's post-hoc test were performed as statistical analyses.

Figure 5. Neonatal induction of intestinal *G6pc1* improves neonatal leptin sensitivity. (**a**) Plasma leptin levels in P9 and P20 and (**b**) hypothalamic basal STAT3 phosphorylation levels in P9 I.G6pc$^{overexp\text{-}P1}$ (white squares) and control littermates (black squares) (mean ± SEM; n= 6-7). (**c**) Correlation between hypothalamic STAT3 phosphorylation and intestinal *G6pc1* expression (**d**) Correlation between hypothalamic STAT3 phosphorylation and plasma leptin levels. (**e**) Representative confocal images and (**f**) quantification of P-STAT3 positive cells in the ARH of P15 pups (mean ± SEM; n= 4-5). Scale bar = 100µm. (**g**) Hypothalamic STAT3 phosphorylation levels after an intraperitoneal leptin injection (mean ± SEM; n= 6-7). T tests were performed as statistical analyses for a, b, f, g and correlation analyses for c and d. *p<0.05.

Figure 6. Neonatal induction of intestinal *G6pc1* protects the metabolism of adult mice fed a hypercaloric diet. Analyses were performed in adult I.G6pc$^{overexp\text{-}P1}$ (white squares) and control littermates (black squares) fed a HFHS diet since the 6th week of life (mean ± SEM; n= 6-7). (**a**) Weight gain. (**b**) Body fat mass and (**c**) body lean mass (% of total body weight). (**d**) Energy expenditure normalized to lean mass. (**e**) Glucose tolerance test with corresponding AUC. (**f**) Insulin tolerance test with corresponding AUC. (**g**) Plasma insulin and (**h**) plasma leptin levels. (**i**) Hypothalamic STAT3 phosphorylation levels. (**j**) Intestinal *G6pc1* mRNA levels relative to control values. (**k**) Intestinal G6Pase activity. Two-way ANOVA, followed by multiple comparisons and Sidak's post hoc test were performed as statistical analyses for weight gain, glucose and insulin tolerance tests. T-tests were performed for others. *p<0.05; **p<0.01; ***p<0.001.

Figure 7. Induction of intestinal *G6pc1* at P12 fails to protect the metabolism of adult mice fed a hypercaloric diet. Analyses were performed in adult I.G6pc$^{overexp\text{-}P12}$ (white lozenges) and control littermates (black lozenges) fed a HFHS diet since the 6th week of life (mean ± SEM, n= 6-7). (**a**) Weight gain. (**b**) Body fat mass and (**c**) body lean mass (% of total body weight). (**d**) Energy expenditure normalized to lean mass. (**e**) Glucose tolerance test with corresponding AUC. (**f**) Insulin tolerance test with corresponding AUC. (**g**) Plasma insulin and (**h**) plasma leptin levels. (**i**) Hypothalamic STAT3 phosphorylation levels. (**j**) Intestinal *G6pc1* mRNA levels relative to control values. (**k**) Intestinal G6Pase activity. Two-way ANOVA, followed by multiple comparisons and Sidak's post hoc test were performed as statistical

analyses for weight gain, glucose and insulin tolerance tests. T-tests were performed for others. *p<0.05; **p<0.01; ***p<0.001.

Figure 8. Neonatal induction of intestinal *G6pc1* controls adipose tissue sympathetic innervation in adult and pups. Representative brightfield images and quantification of adipocytes per (**a**) iWAT and (**b**) epiWAT area on adipose tissue histological sections of adult I.G6pc$^{overexp\text{-}P1}$ (white squares) and control littermates (black squares) fed a HFHS diet since the 6th week of life (mean ± SEM; n= 5-6). Scale bar = 100µm. Representative western blot images and relative TH levels in the (**c**) iWAT, (**d**) epiWAT and (**e**) BAT of adult I.G6pc$^{overexp\text{-}P1}$ (white squares) and control littermates (black squares) fed a HFHS diet since the 6th week of life (mean ± SEM; n= 5-7). (**f**) Ucp1 expression levels in BAT of adult I.G6pc$^{overexp\text{-}P1}$ (white squares) and control littermates (black squares) fed a HFHS diet since the 6th week of life (mean ± SEM; n= 7-8). Representative western blot images and relative TH levels in the (**g**) iWAT, (**h**) epiWAT and (**i**) BAT of adult I.G6pc$^{overexp\text{-}P12}$ (white lozenges) and control littermates (black lozenges) fed a HFHS diet since the 6th week of life (mean ± SEM; n= 5). Representative western blot images and relative TH levels in the (**j**) iWAT and (**k**) BAT of I.G6pc$^{overexp\text{-}P1}$ (white squares) and control littermate (black squares) (mean ± SEM; n= 4-6). Representative western blot images and relative TH levels in the (**l**) iWAT, (**m**) epiWAT (*=outlier) and (**n**) BAT of I.G6pc$^{overexp\text{-}c}$ (white circles) and control littermate P15-pups (black circles) (mean ± SEM; n= 7). T-tests were performed as statistical analyses. *p<0.05, ***p<0.001.

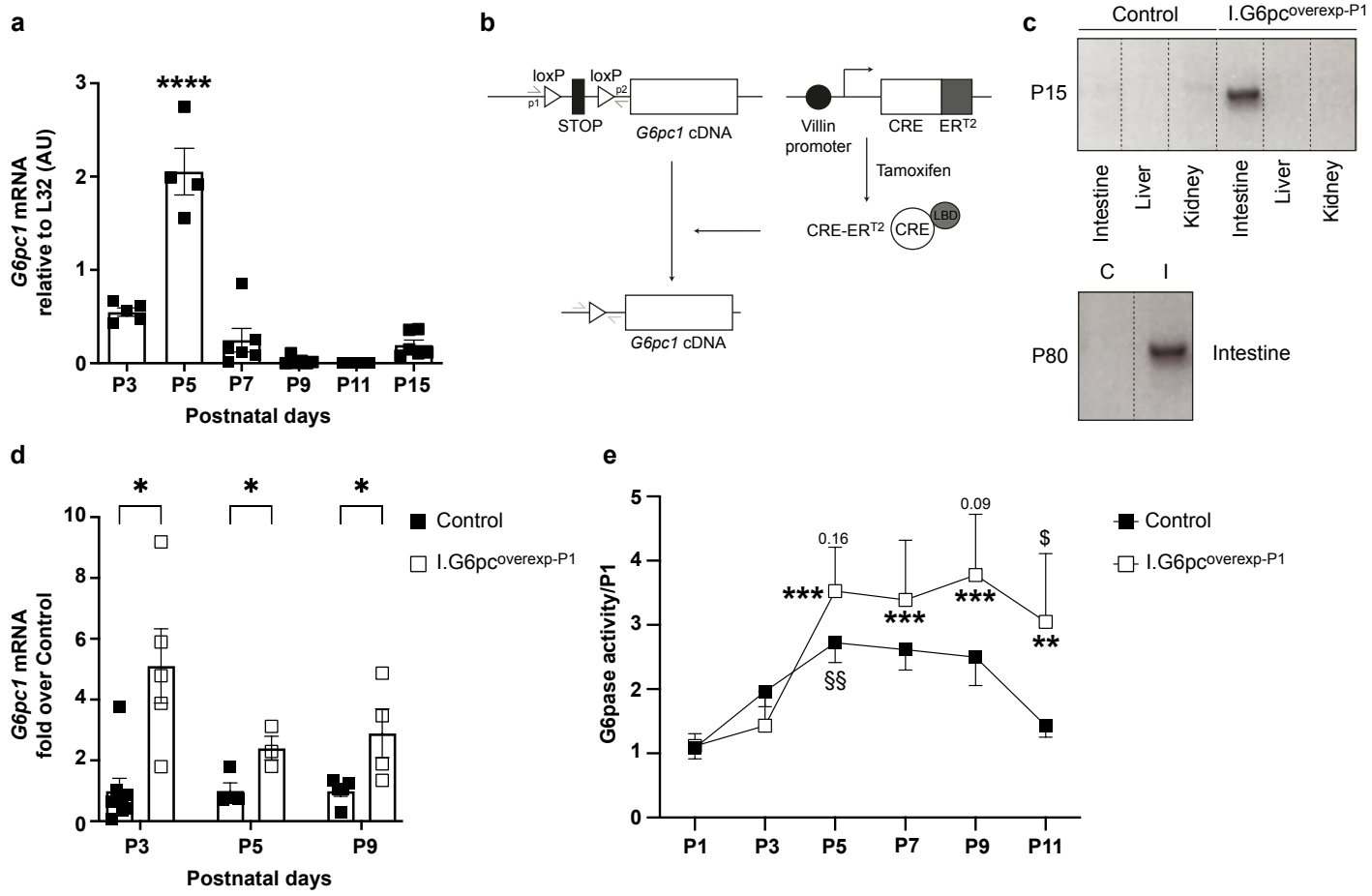
a
G6pc1 mRNA relative to L32 (AU)
****
P3
P5
P7
P9
P11
P15
Postnatal days
b
loxP
loxP
p1
p2
STOP
G6pc1 cDNA
Villin promoter
CRE
ERT2
Tamoxifen
CRE-ERT2
LBD
G6pc1 cDNA
c
Control
I.G6pcoverexp-P1
P15
Intestine
Liver
Kidney
C
I
P80
Intestine
d
G6pc1 mRNA fold over Control
Control
I.G6pcoverexp-P1
Postnatal days
e
G6pase activity/P1
0.16
0.09
$
§§
P1
P3
P5
P7
P9
P11

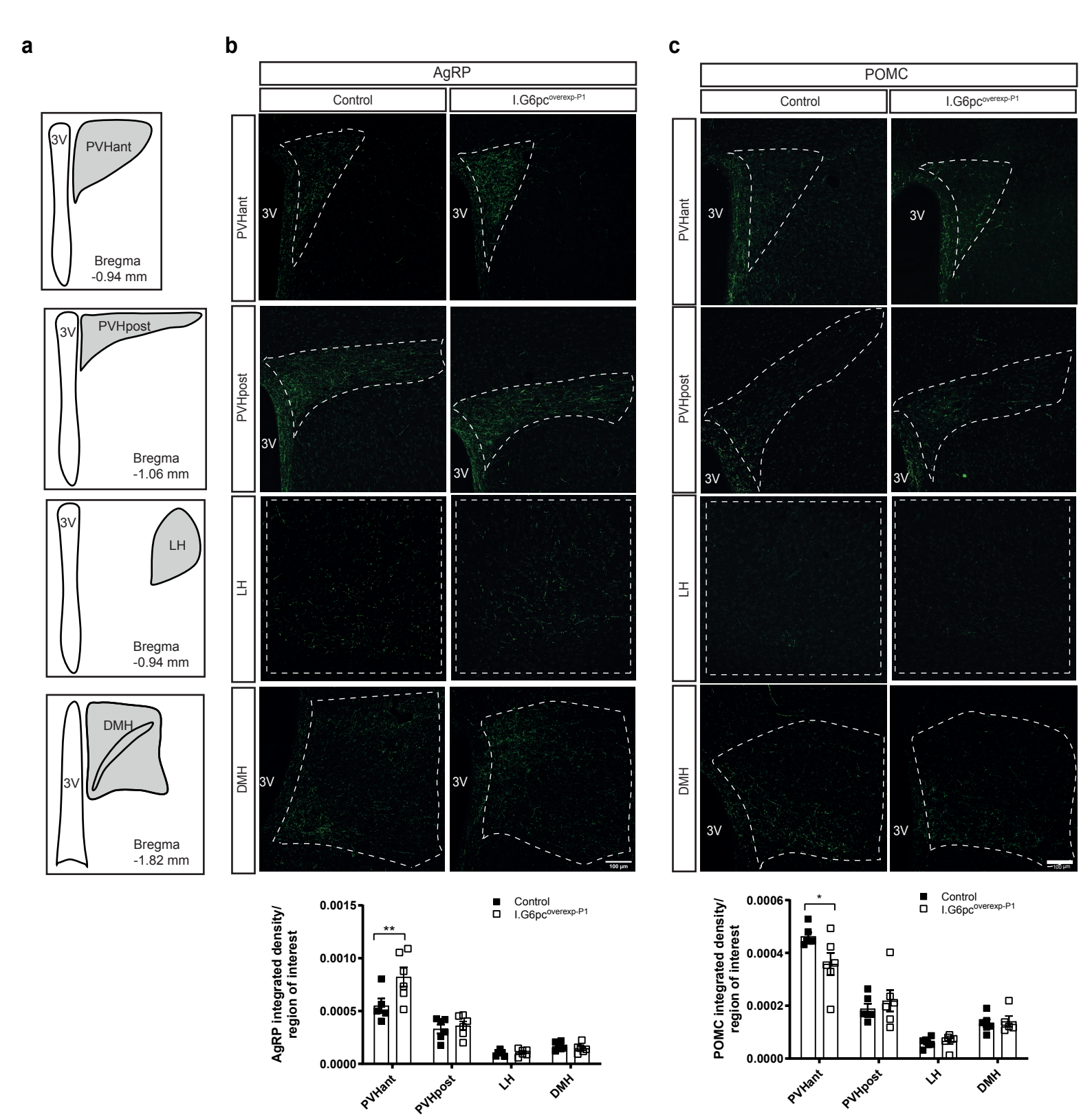
a
b
c
AgRP
POMC
Control
I.G6pc overexp-P1
PVHant
PVHpost
LH
DMH
3V
Bregma
-0.94 mm
Bregma
-1.06 mm
Bregma
-0.94 mm
Bregma
-1.82 mm
100 µm
AgRP integrated density/
region of interest
POMC integrated density/
region of interest
0.0015
0.0010
0.0005
0.0000
0.0006
0.0004
0.0002
0.0000
**
*

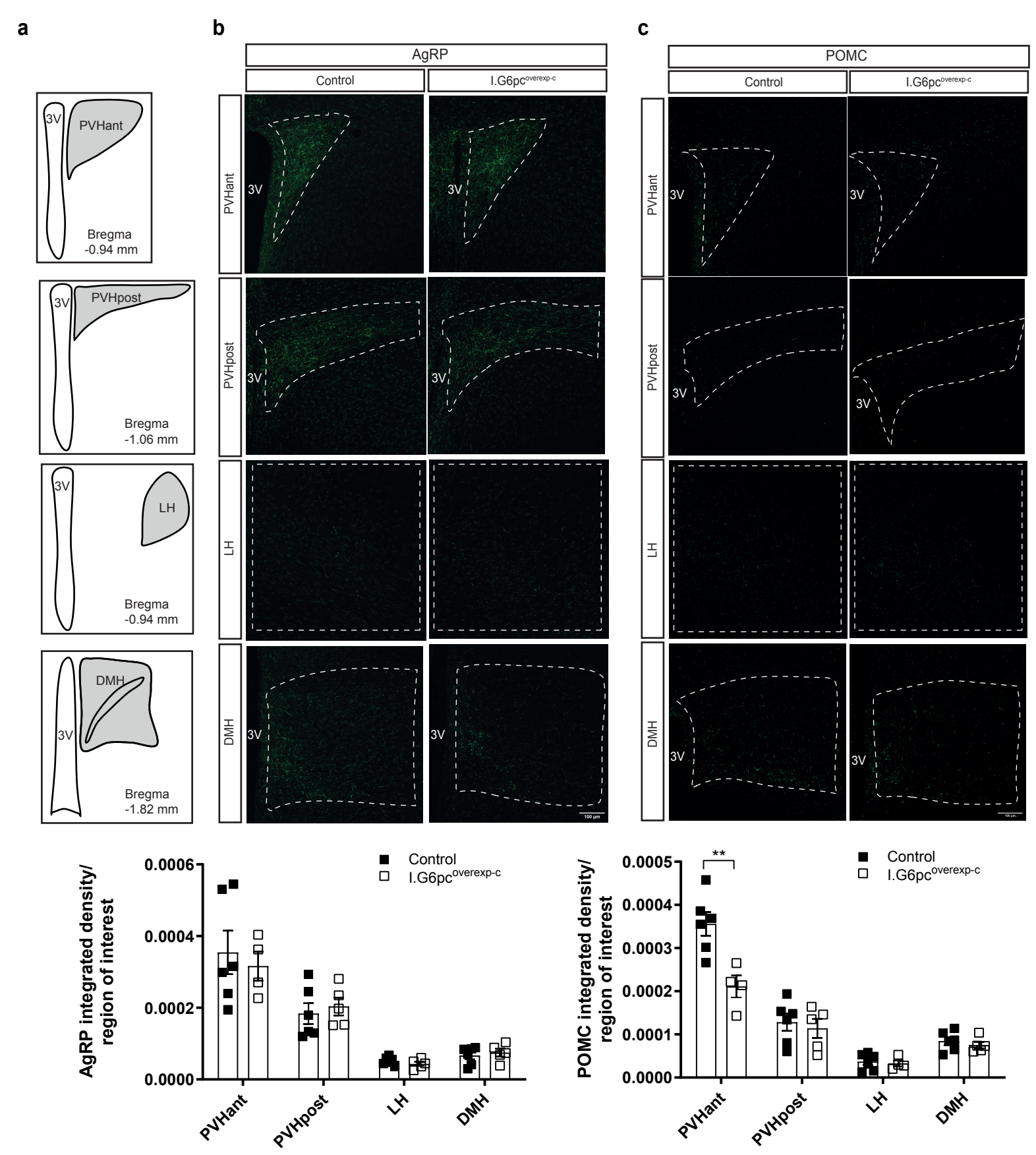
a
b
c
AgRP
POMC
Control
I.G6pc overexp-c
PVHant
PVHpost
LH
DMH
3V
Bregma
-0.94 mm
Bregma
-1.06 mm
Bregma
-0.94 mm
Bregma
-1.82 mm
100 µm

AgRP integrated density/
region of interest
0.0006
0.0004
0.0002
0.0000
Control
I.G6pc overexp-c
PVHant
PVHpost
LH
DMH

POMC integrated density/
region of interest
0.0005
0.0004
0.0003
0.0002
0.0001
0.0000
**
Control
I.G6pc overexp-c
PVHant
PVHpost
LH
DMH

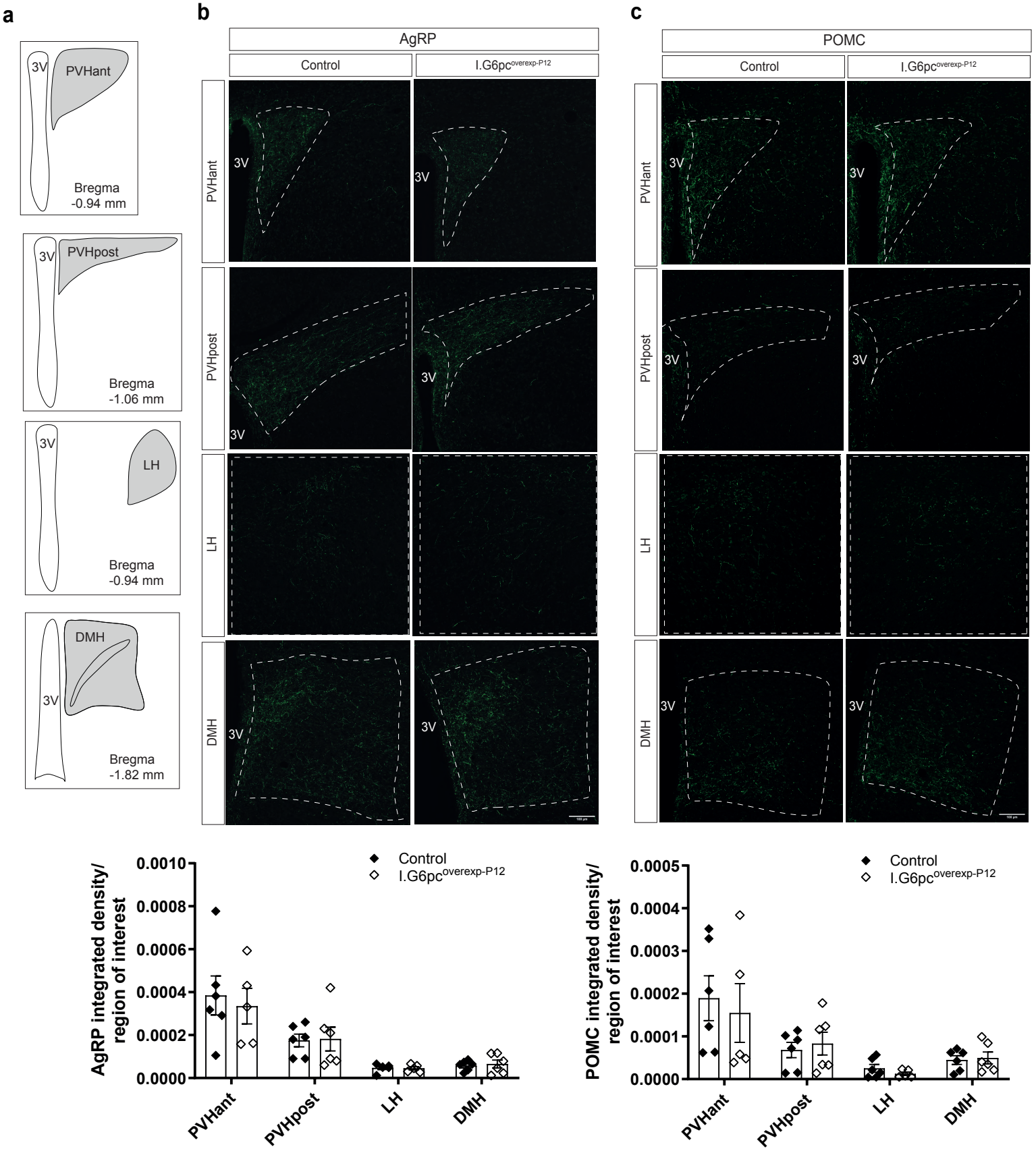
a
3V
PVHant
Bregma
-0.94 mm
3V
PVHpost
Bregma
-1.06 mm
3V
LH
Bregma
-0.94 mm
3V
DMH
Bregma
-1.82 mm
b
AgRP
Control
I.G6pc overexp-P12
PVHant
PVHpost
LH
DMH
3V
c
POMC
Control
I.G6pc overexp-P12
PVHant
PVHpost
LH
DMH
3V
AgRP integrated density/
region of interest
0.0010
0.0008
0.0006
0.0004
0.0002
0.0000
Control
I.G6pc overexp-P12
PVHant
PVHpost
LH
DMH
POMC integrated density/
region of interest
0.0005
0.0004
0.0003
0.0002
0.0001
0.0000
Control
I.G6pc overexp-P12
PVHant
PVHpost
LH
DMH

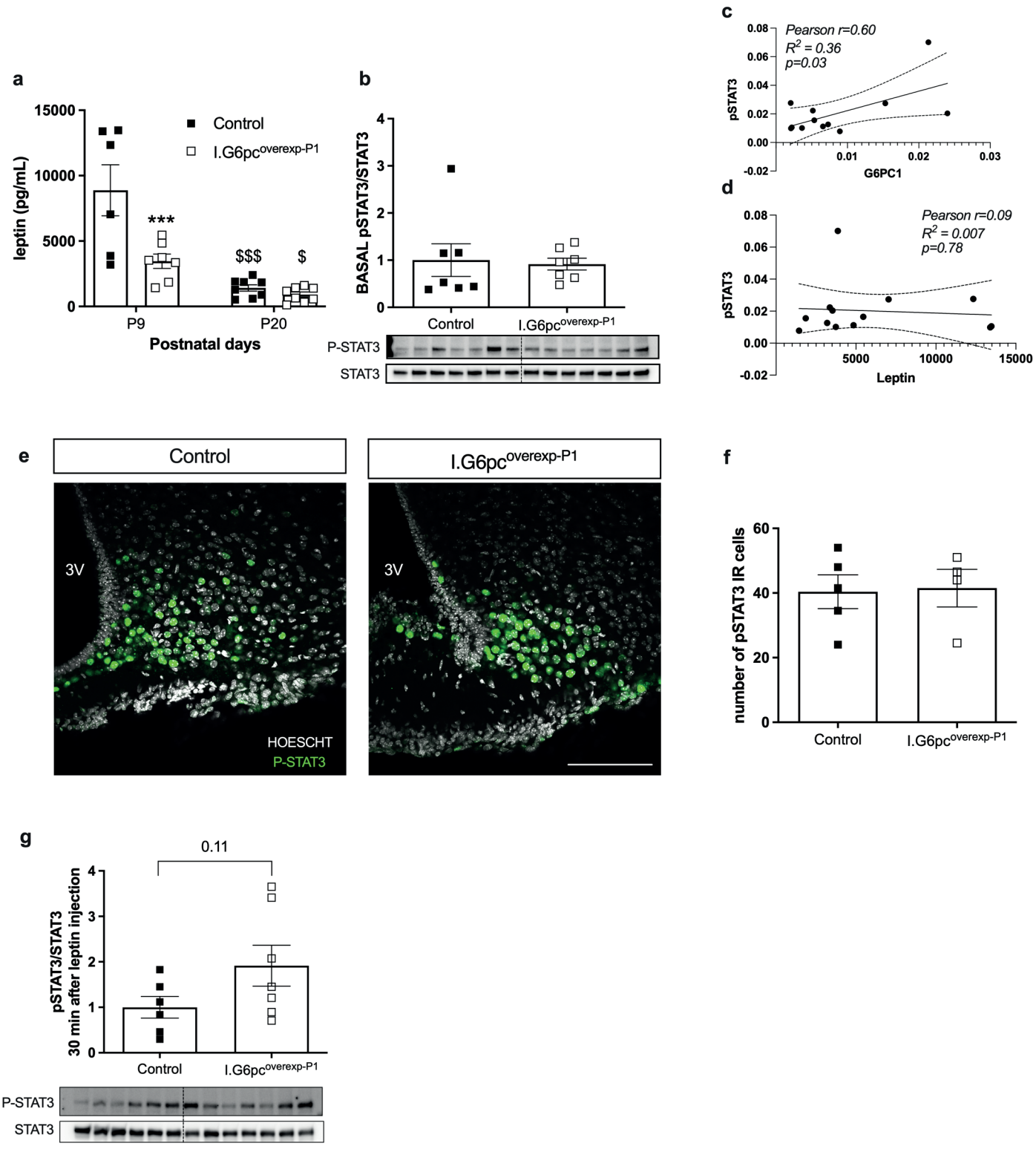
a
leptin (pg/mL)
15000
10000
5000
0
Control
I.G6pc^overexp-P1
***
$$$
$
P9
P20
Postnatal days
b
BASAL pSTAT3/STAT3
4
3
2
1
0
Control
I.G6pc^overexp-P1
P-STAT3
STAT3
c
Pearson r=0.60
R² = 0.36
p=0.03
pSTAT3
0.08
0.06
0.04
0.02
0.00
-0.02
0.01
0.02
0.03
G6PC1
d
Pearson r=0.09
R² = 0.007
p=0.78
pSTAT3
0.08
0.06
0.04
0.02
0.00
-0.02
5000
10000
15000
Leptin
e
Control
I.G6pc^overexp-P1
3V
3V
HOESCHT
P-STAT3
f
number of pSTAT3 IR cells
60
40
20
0
Control
I.G6pc^overexp-P1
g
0.11
pSTAT3/STAT3
30 min after leptin injection
4
3
2
1
0
Control
I.G6pc^overexp-P1
P-STAT3
STAT3

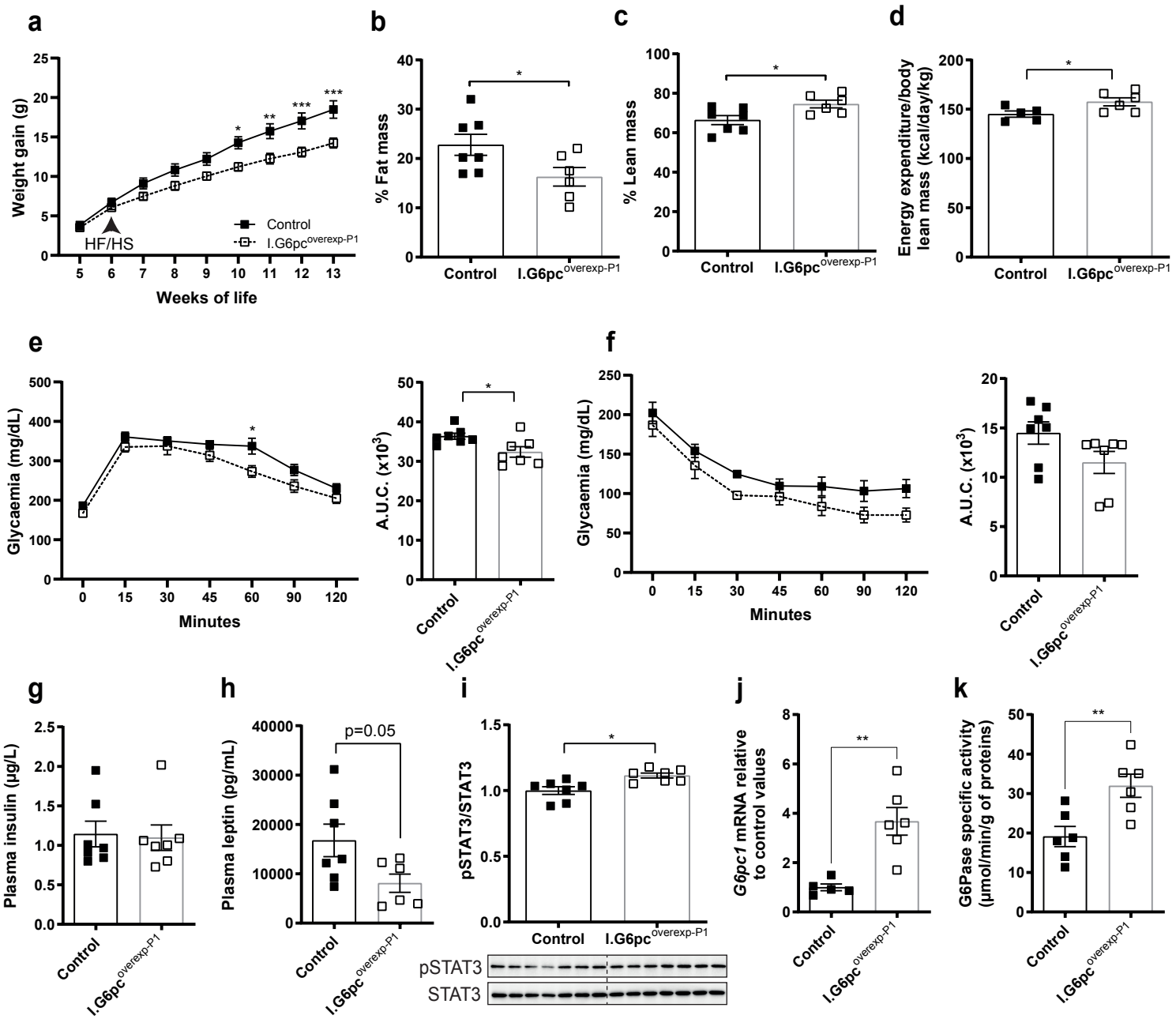
a
Weight gain (g)
Weeks of life
HF/HS
Control
I.G6pc overexp-P1
b
% Fat mass
c
% Lean mass
d
Energy expenditure/body lean mass (kcal/day/kg)
e
Glycaemia (mg/dL)
Minutes
A.U.C. (x10³)
f
Glycaemia (mg/dL)
Minutes
A.U.C. (x10³)
g
Plasma insulin (µg/L)
h
Plasma leptin (pg/mL)
p=0.05
i
pSTAT3/STAT3
pSTAT3
STAT3
j
G6pc1 mRNA relative to control values
k
G6Pase specific activity (µmol/min/g of proteins)

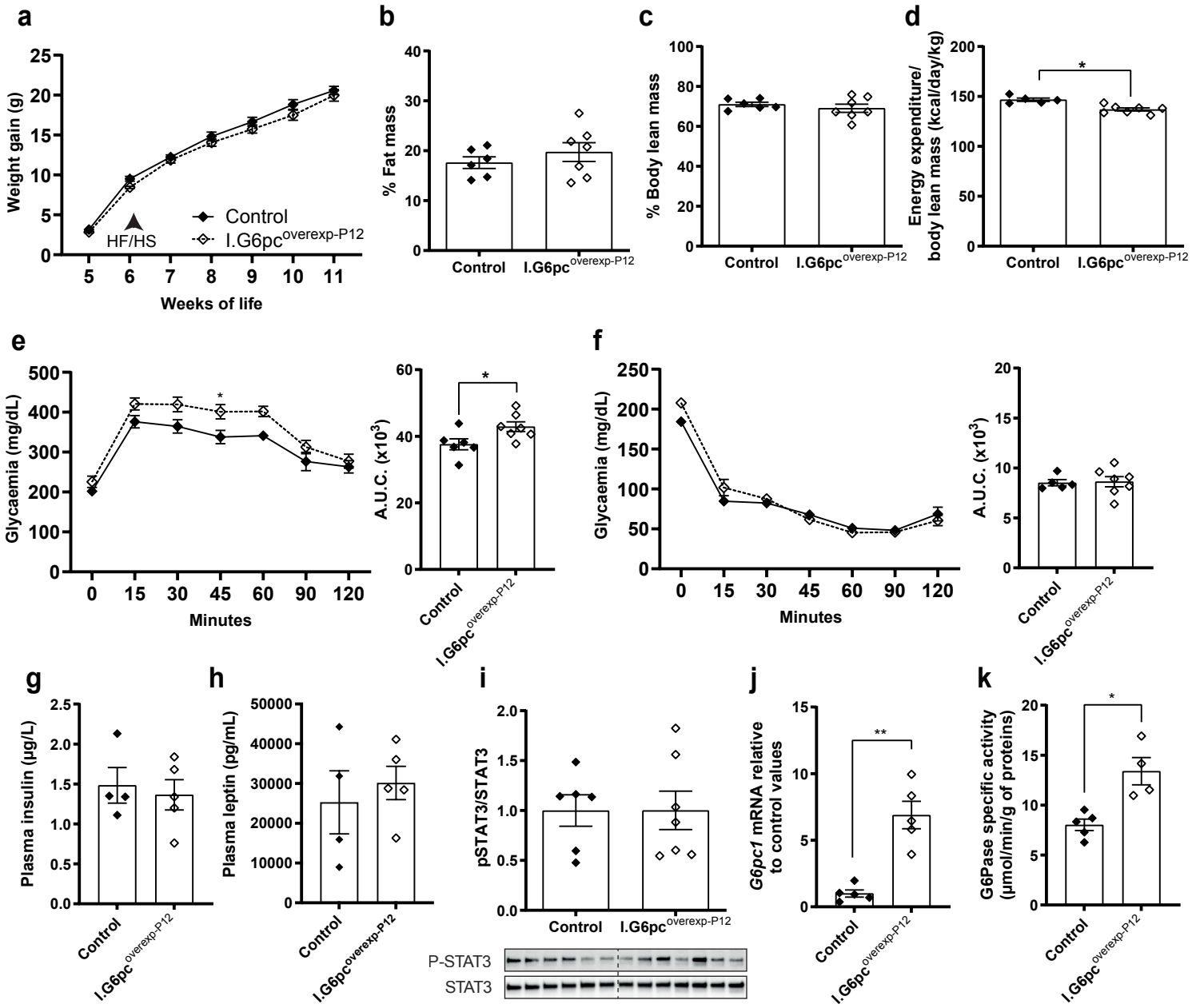
a
Weight gain (g)
Weeks of life
HF/HS
Control
I.G6pc overexp-P12
b
% Fat mass
c
% Body lean mass
d
Energy expenditure/ body lean mass (kcal/day/kg)
e
Glycaemia (mg/dL)
Minutes
A.U.C. (x10³)
f
Glycaemia (mg/dL)
Minutes
A.U.C. (x10³)
g
Plasma insulin (µg/L)
h
Plasma leptin (pg/mL)
i
pSTAT3/STAT3
P-STAT3
STAT3
j
G6pc1 mRNA relative to control values
k
G6Pase specific activity (µmol/min/g of proteins)

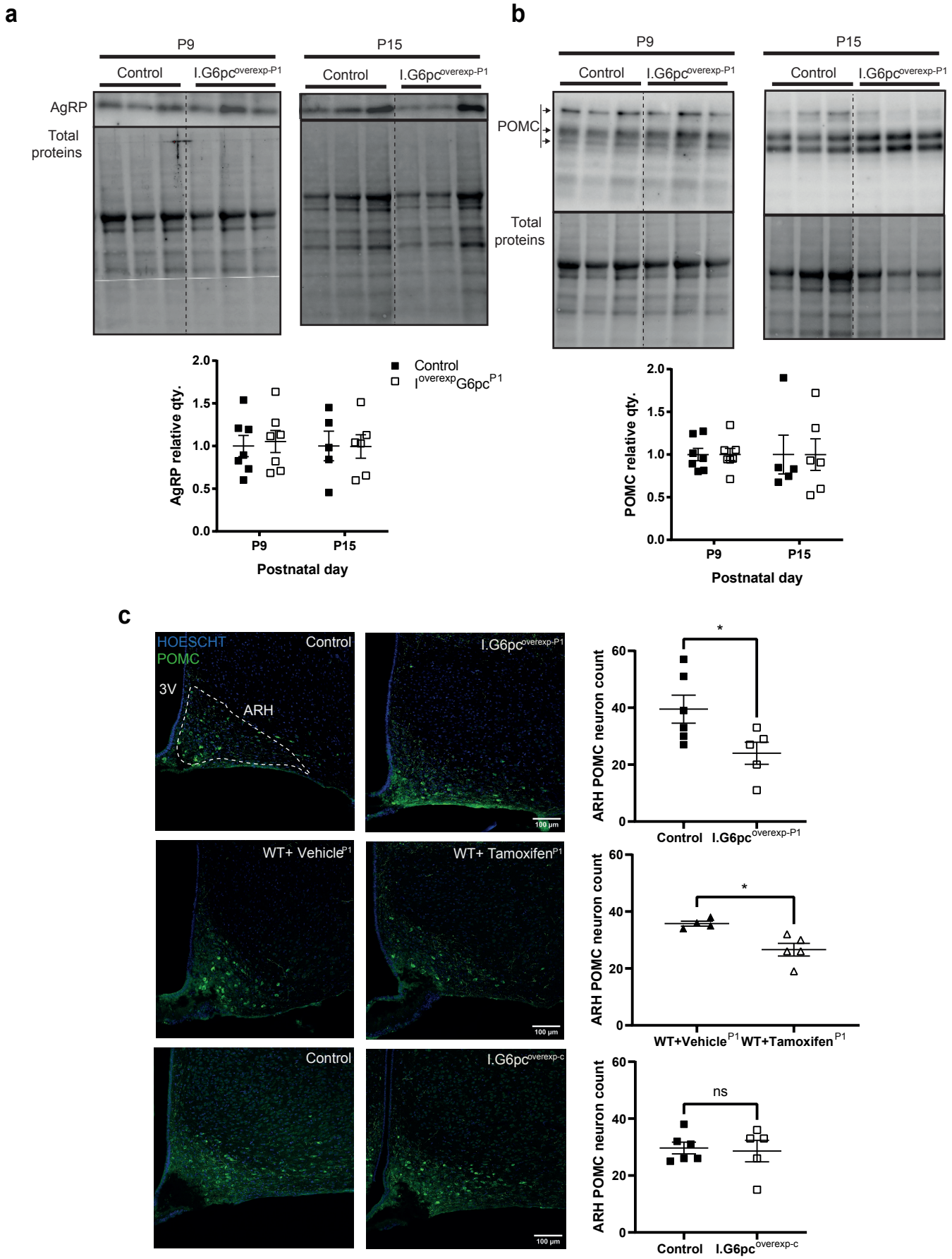

Supplemental Fig.1 : Impact of the neonatal induction of G6pc1 on AgRP and POMC protein amount and on the number of ARH POMC neurons.

(a-b) Representative western blot images and relative AgRP and POMC levels in the hypothalamus of I.G6pc$^{overexp\text{-}P1}$ and control pups aged of 9 and 15 days, respectively (mean ± SEM; n=5-7). (c) Representative confocal ARH images and quantification of POMC-immunoreactive cells of P20 I.G6pc$^{overexp\text{-}P1}$ and control littermates (mean ± SEM; n=5-6), P20 WT mice injected with tamoxifen or vehicle at P1 (mean ± SEM; n=4-5), and P20 I.G6pc$^{overexp\text{-}c}$ and control littermates (mean ± SEM; n=5-6). Scale bar = 100µm. P: postnatal day; 3V: 3rd ventricle; ARH: arcuate nucleus of the hypothalamus. Panels a-b: 2-way ANOVA, followed by multiple comparisons and Sidak's post hoc test; Panel c: T-tests. *p<0.05.

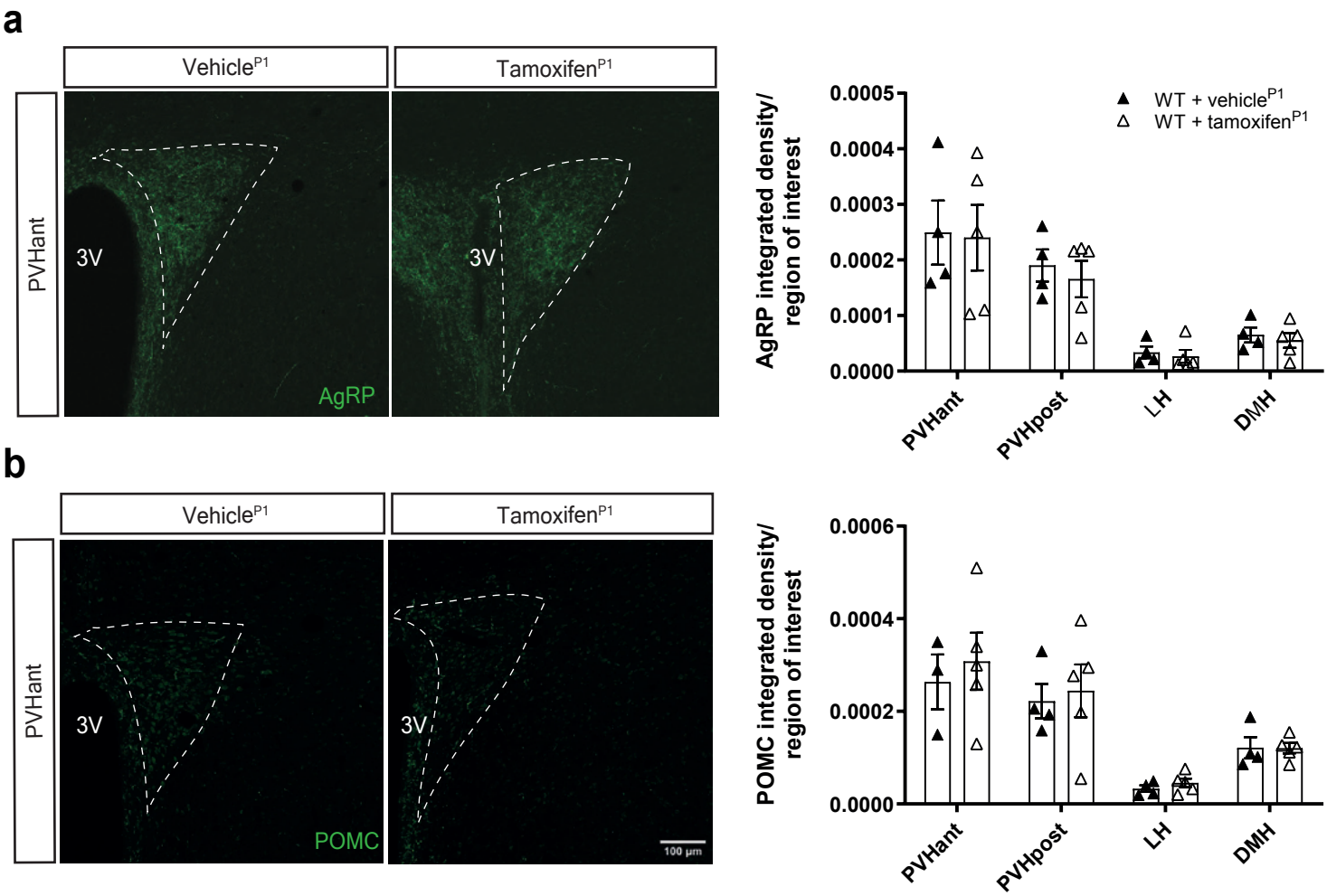

Supplemental Fig. 2: Tamoxifen treatment of P1 pups has no effect on the development of AgRP and POMC neural projections. (a) Representative confocal PVNant images and quantification of AgRP-immunoreactive fibers of P20 wild type pups treated with tamoxifen (white triangles) or vehicle (black triangles) at P1 (mean ± SEM; n= 4-5). (b) Representative confocal PVNant images and quantification of POMC-immunoreactive fibers of P20 wild type pups treated tamoxifen (white triangles) or vehicle (black triangles) at P1 (mean ± SEM; n= 3-5). Scale bar = 100µm P: postnatal day; 3V: 3rd ventricle; PVHant: anterior part of the paraventricular nucleus; PVHpost: posterior part of the paraventricular nucleus; LH: lateral hypothalamic area; DMH: dorsomedial nucleus. Two-way ANOVA, followed by multiple comparisons and Sidak's post hoc test were performed as statistical analyses.

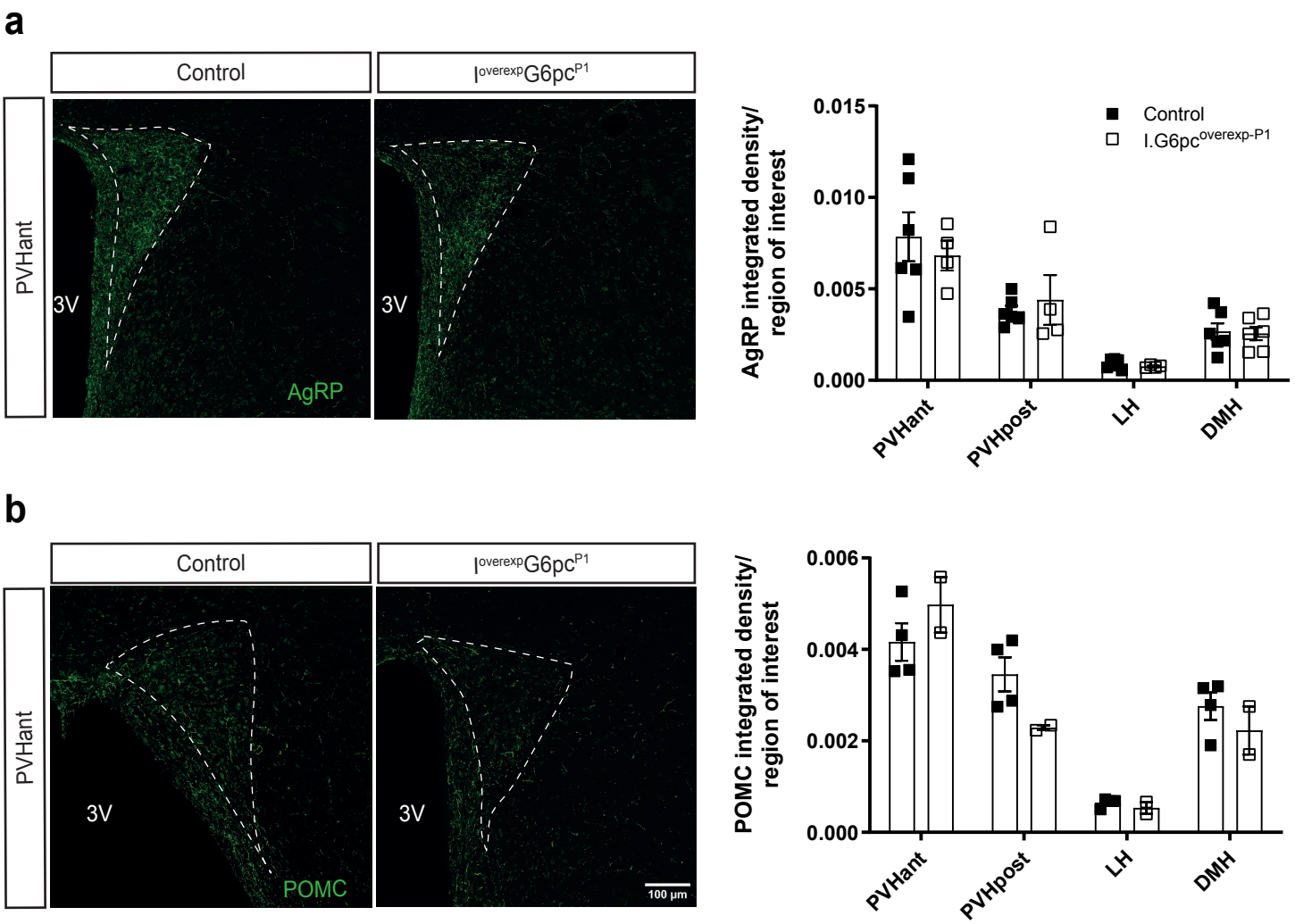

Supplemental Fig. 3: AgRP and POMC neural projections normalized in adult I.G6pc$^{overexp-P1}$ mice. (a) Representative confocal PVNant images and quantification of AgRP-immunoreactive fibers of P80 I.G6pc$^{overexp-P1}$ (white squares) and control littermates (black squares) (mean ± SEM; n= 5-6). (b) Representative confocal PVNant images and quantification of POMC-immunoreactive fibers of P80 I.G6pc$^{overexp-P1}$ (white squares) and control littermates (black squares) (mean ± SEM; n= 2-4). Scale bar = 100µm . P: postnatal day; 3V: 3rd ventricle; PVHant: anterior part of the paraventricular nucleus; PVHpost: posterior part of the paraventricular nucleus; LH: lateral hypothalamic area; DMH: dorsomedial nucleus. Two-way ANOVA, followed by multiple comparisons and Sidak's post hoc test were performed as statistical analyses.

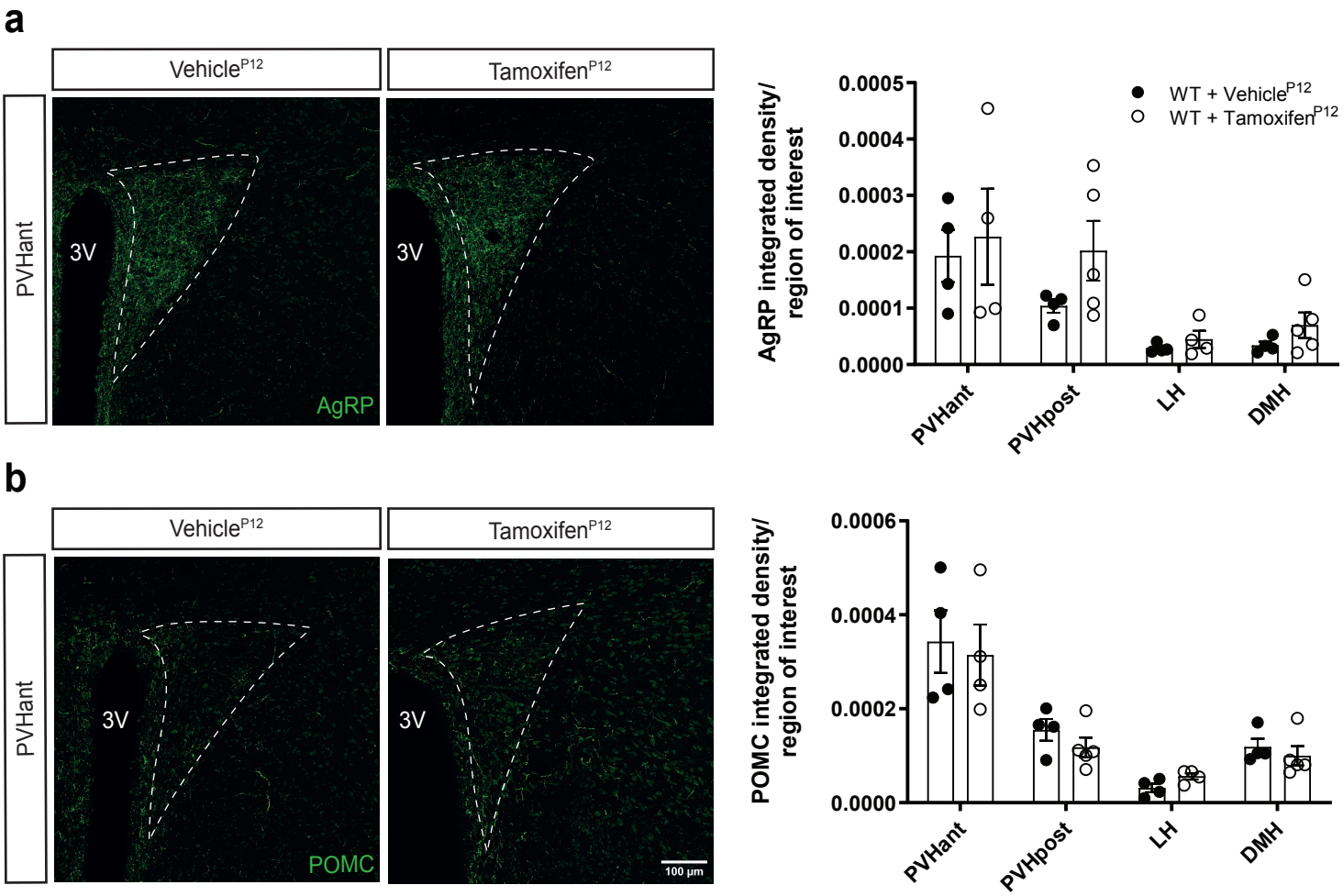

Supplemental Fig. 4: Tamoxifen treatment at P12 has no effect on the development of AgRP and POMC neural projections. (a) Representative confocal PVNant images and quantification of AgRP-immunoreactive fibers of P20 wild type pups treated with tamoxifen (white circles) or vehicle (black circles) at P12 (mean ± SEM; n= 4-5). (b) Representative confocal PVNant images and quantification of POMC-immunoreactive fibers of P20 wild type pups treated with tamoxifen (white circles) or vehicle (black circles) at P12 (mean ± SEM; n= 4). Scale bar = 100µm P: postnatal day; 3V: 3rd ventricle; PVHant: anterior part of the paraventricular nucleus; PVHpost: posterior part of the paraventricular nucleus; LH: lateral hypothalamic area; DMH: dorsomedial nucleus. Two-way ANOVA, followed by multiple comparisons and Sidak's post hoc test were performed as statistical analyses.

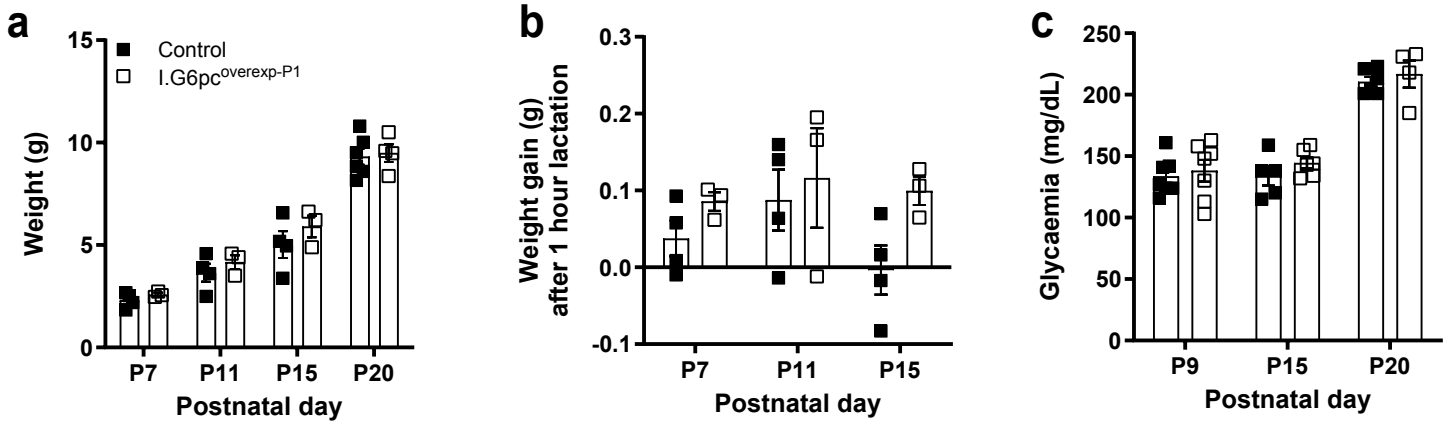

Supplemental Fig. 5: Normal weight and glycaemia in pups with a neonatal induction of intestinal gluconeogenesis. (a) Neonatal weight (mean ± SEM; n= 3-6). (b) Weight gain after pups were reunited with dams for 1 hour (mean ± SEM; n= 3-4). (c) Neonatal glycaemia (mean ± SEM; n= 4-7). P: postnatal day. Two-way ANOVA, followed by multiple comparisons and Sidak's post hoc test were performed as statistical analyses.

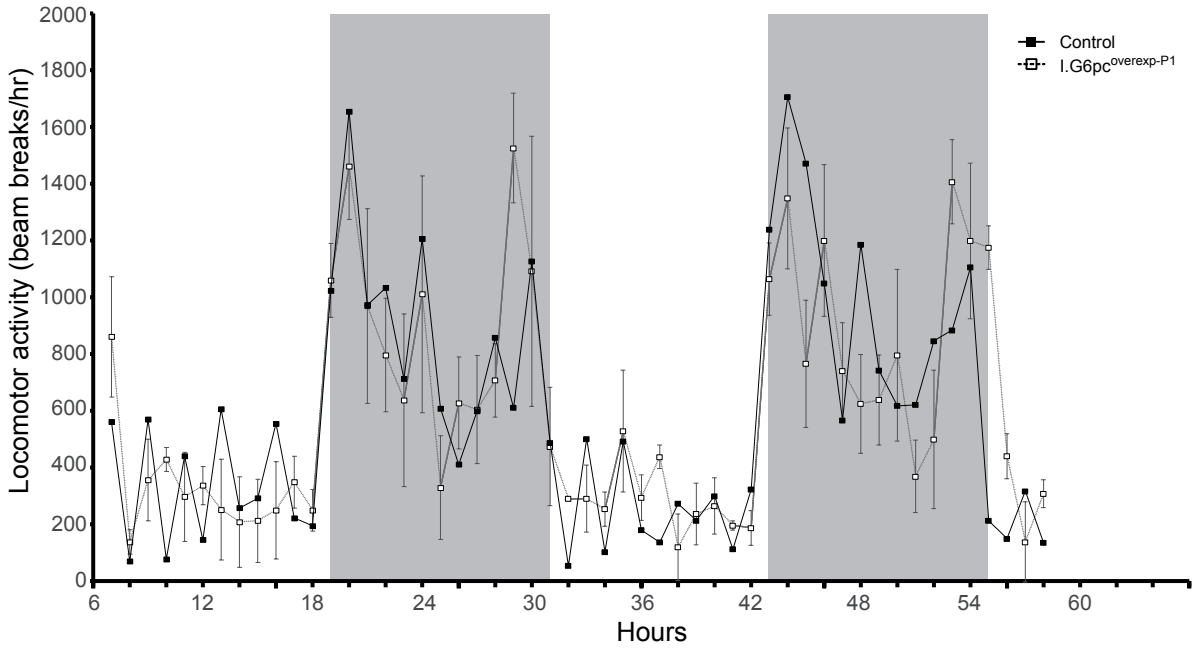

Supplemental Fig. 6: Hourly locomotor activity values of I.G6pc$^{overexp-P1}$ (white squares) and their control littermates (black squares) measured during the second (from 7 AM) and third day of housing in indirect calorimetric cages (mean ± SEM; n= 5-6).

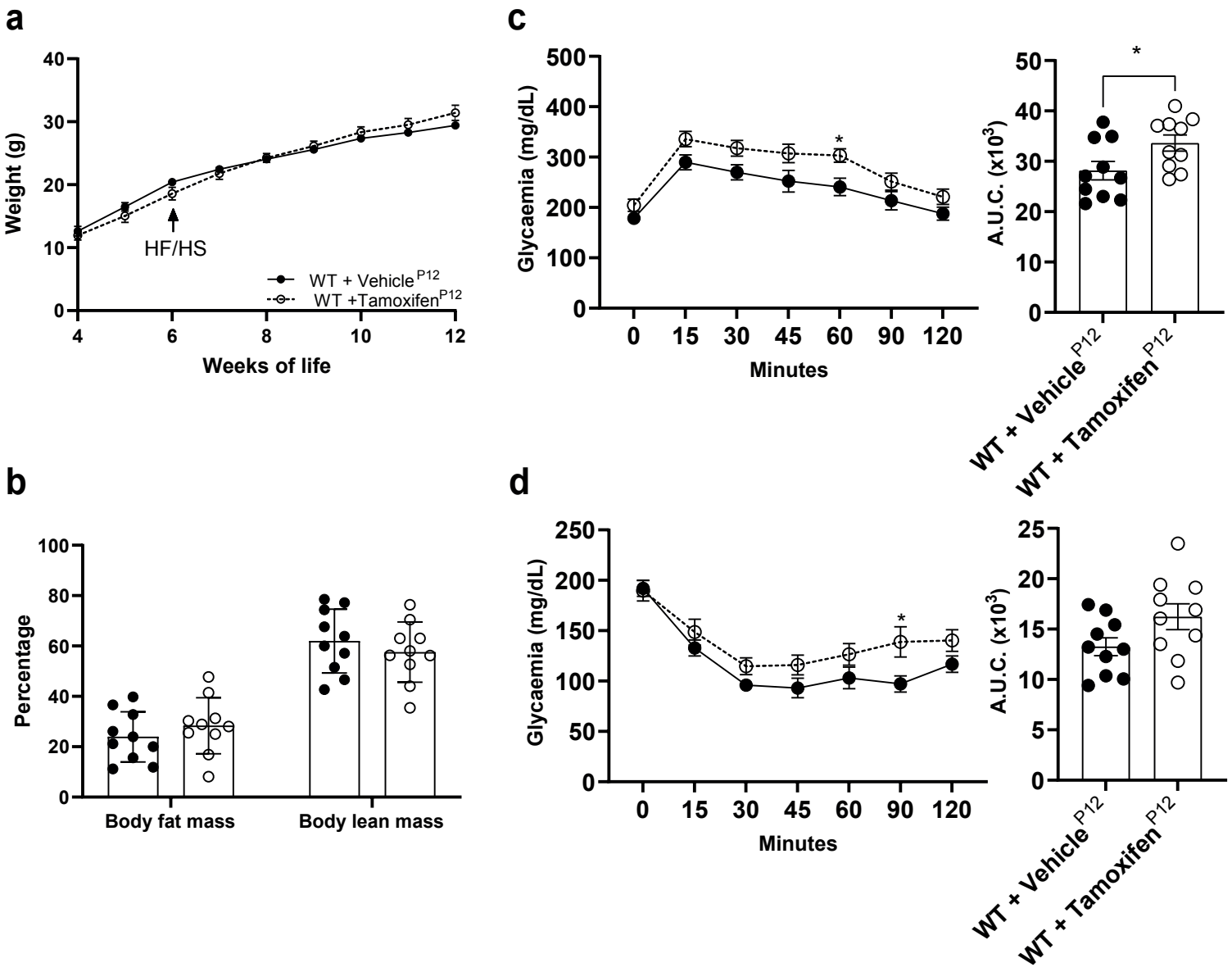

Supplemental Fig. 7. Tamoxifen treatment at P12 has no effect on the metabolism of adult mice fed a hypercaloric diet. Analyses were performed in adult wild-type treated with Tamoxifen (white circles) or with Vehicle (black circles) at P12 and fed a HFHS diet since the 6th week of life (mean ± SEM, n= 9-10). (a) Weight gain. (b) Body fat mass and body lean mass (% of total body weight). (c) Glucose tolerance test with corresponding AUC. (d) Insulin tolerance test with corresponding AUC. Two-way ANOVA, followed by multiple comparisons and Sidak's post hoc test were performed as statistical analyses for weight gain, glucose and insulin tolerance tests. T-tests were performed for body composition. *p<0.05.

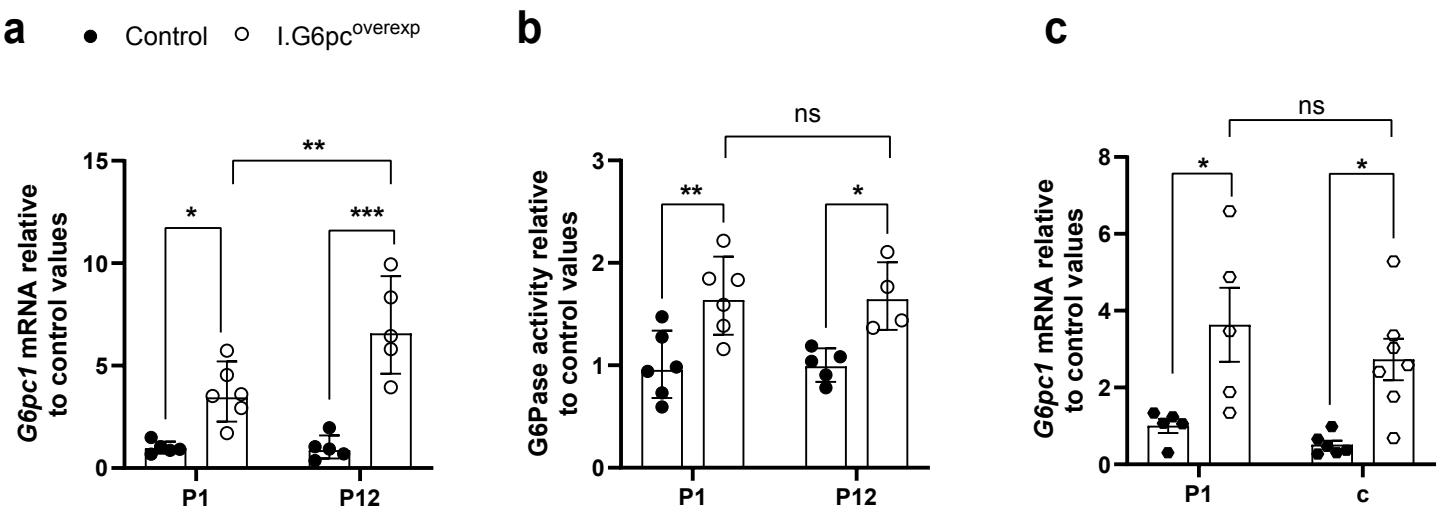

Supplementary Fig. 8: The expression of *G6pc1* is similarly induced in the different mouse models used. (a) Expression of *G6pc1* relative to the respective littermate values (black circles) of I.G6pc$^{overexp\text{-}P1}$ and I.G6pc$^{overexp\text{-}P12}$ mice (white circles) (mean ± SEM; n= 4-6). (b) G6Pase activity (µmol/min/g of protein) relative to the respective littermate values (black circles) of I.G6pc$^{overexp\text{-}P1}$ and I.G6pc$^{overexp\text{-}P12}$ mice (white circles) (mean ± SEM; n= 4-6). (c) Expression of *G6pc1* relative to the respective littermate values (black circles) of I.G6pc$^{overexp\text{-}P1}$ and I.G6pc$^{overexp\text{-}c}$ mice (white circles) (mean ± SEM; n= 5-7). Two-way ANOVA, followed by multiple comparisons and Tukey's post hoc test were performed as statistical analyses.